

# InfoBound: A Provable Information-Bounds Inspired Framework for Both OoD Generalization and OoD Detection

Lin Zhu, Yifeng Yang, Zichao Nie, Yuan Gao, Jiarui Li, Qinying Gu, Xinbing Wang, *Senior Member, IEEE*, Chenghu Zhou, Nanyang Ye

arXiv:2504.09448v1 [cs.CV] 13 Apr 2025

**Abstract**—In real-world scenarios, distribution shifts give rise to the importance of two problems: out-of-distribution (OoD) generalization, which focuses on models’ generalization ability against covariate shifts (i.e., the changes of environments), and OoD detection, which aims to be aware of semantic shifts (i.e., test-time unseen classes). Real-world testing environments often involve a combination of both covariate and semantic shifts. While numerous methods have been proposed to address these critical issues, only a few works tackled them simultaneously. Moreover, prior works often improve one problem but sacrifice the other. To overcome these limitations, we delve into boosting OoD detection and OoD generalization from the perspective of information theory, which can be easily applied to existing models and different tasks. Building upon the theoretical bounds for mutual information and conditional entropy, we provide a unified approach, composed of Mutual Information Minimization (MI-Min) and Conditional Entropy Maximizing (CE-Max). Extensive experiments and comprehensive evaluations on multi-label image classification and object detection have demonstrated the superiority of our method. It successfully mitigates trade-offs between the two challenges compared to competitive baselines.

**Index Terms**—OoD generalization, OoD detection, Mutual information, Conditional entropy, Bound minimization.

## 1 INTRODUCTION

Machine learning models deployed in real-world settings often encounter out-of-distribution (OoD) challenges, which stem from disparities in data distributions between the training and test sets [1], [2]. Consequently, models can encounter known classes living in diverse environments, as well as unseen classes. Real-world testing environments typically involve a combination of these two types of distribution shifts [3], emphasizing the need for models to handle them simultaneously. These two types of distribution shifts are referred to as *covariate shift* (i.e., changes in the

Lin Zhu, Yifeng Yang, Yuan Gao, Jiarui Li, Xinbing Wang, Chenghu Zhou Nanyang Ye are with the Shanghai Jiao Tong University, Shanghai 200240, China (e-mail: zhulin\_sjtu@sjtu.edu.cn; maxwellquadyang@gmail.com; yogggy23@sjtu.edu.cn, kingdom-of-warriors@sjtu.edu.cn, xwang8@sjtu.edu.cn; zhouchsjtu@gmail.com; ynylincoln@sjtu.edu.cn); Zichao Nie is with Beijing Jiaotong University, Beijing, 100044, China, e-mail: niezichao@bupt.edu.cn. Qinying Gu is with Shanghai Artificial Intelligence Laboratory, Shanghai, 200000, China, e-mail: guqinying@pjlab.org.cn. Nanyang Ye is the corresponding author.

This work is still ongoing and will be updated.

Data	In-Distribution	Covariate Shift	Semantic Shift
Image Classification			
Ideal Result	* OoD Detection: Semantic IN * Classification: Cow	* OoD Detection: Semantic IN * Classification: Cow	* OoD Detection: Semantic OUT * Do Not Perform Classification
Object Detection			
Ideal Result	* OoD Detection: Semantic IN * Perform Classification for Predicted Boxes	* OoD Detection: Semantic IN * Perform Classification for Predicted Boxes	* OoD Detection: Semantic OUT * Do Not Perform Classification

Fig. 1: Illustration of three types of data encountered in various tasks when deploying models in the open world: (i) in-distribution data (e.g., driving data in clear weather), (ii) covariate-shifted data (e.g., driving data in rainy weather), and (iii) semantic-shifted data (e.g., hippopotamus). Leveraging the labeled in-distribution (ID) data and the freely available unlabeled OoD data, our framework improved both OoD generalization and OoD detection.

environment) and *semantic shift* (i.e., unseen classes at test time), highlighting the importance of addressing two key problems: *OoD generalization*, which focuses on the model’s ability to generalize in the presence of covariate shifts, and *OoD detection*, which aims to identify unseen classes. By developing learning models that effectively adapt to changing environments and remain aware of unseen classes, we can ensure safety and reliability in real-world applications. See Figure 1 for an illustration depicting the challenges encountered across various tasks.

However, despite numerous methods proposed to address these two critical issues, only a few works simultaneously handle them [3], [4]. For example, a new unified approach [4], namely SCONE, has been proposed to generalize against covariate shifts while robustly detecting semantic shifts simultaneously. Taking advantage of freely available unlabeled data in the wild that captures the environmental

test-time distributions under both covariate and semantic shifts, SCONE utilizes a novel margin-based learning framework to identify in-distribution (ID) data and semantic-shifted OoD data by energy scores.

The SCONE method has creatively improved OoD generalization meanwhile being capable of OoD detection. However, the testing approach used in SCONE needs to be improved in real-world scenarios. When evaluating OoD generalization, SCONE performs classification based on data without mixing in semantic-shifted OoD data. When evaluating OoD detection, SCONE discriminates based on a mixture of ID data and semantic-shifted OoD data, without including covariate-shifted data. In real-world scenarios, datasets often involve combinations of ID, covariate-shifted, and semantic-shifted samples, making it challenging to determine the shift categories of individual samples without prior knowledge. Handling such mixed shifts requires pre-determining which datasets have covariate shifts and which have semantic shifts, and subsequently focusing on classifying the selected datasets with covariate shifts. On the other hand, it is worth noting that SCONE [4], like most previous methods [5], [6], [7], [8], [9], has mainly addressed the two issues in the context of image classification tasks, leaving their performance in other tasks, such as object detection, unexplored. Moreover, although SCONE achieved strong OoD generalization results, it exhibited a non-negligible performance degradation in OoD detection compared to its competitor WOODS [9].

In this paper, we aim to offer a unified solution to tackle the aforementioned challenges, particularly focusing on the trade-off between OoD generalization and OoD detection exhibited in the SCONE method [4]. Initially, we theoretically show that OoD generalization against covariate factors and OoD detection could be treated as two sides of one coin and these two challenging tasks could mutually boost. Motivated by this, building upon carefully established theoretical bounds for mutual information and conditional entropy, we develop an **information-based bounds**-inspired framework called *InfoBound*, designed to enhance both tasks. As shown in Figure 2, following the same data setting as SCONE, the InfoBound method consists of two processes: Mutual Information Minimization (MI-Min) and Conditional Entropy Maximization (CE-Max). In the MI-Min process, we perform representation reshaping by decreasing the inner product among different semantic factors. This step also helps mitigate the influence of covariate shifts thus enhancing OoD generalization. On the other hand, the CE-Max process introduces energy-based regularization to enable the identification of semantic-shifted OoD data. Through the use of comprehensive metrics to evaluate model performance in OoD detection and OoD generalization in real-world scenarios, we have demonstrated that our InfoBound approach outperforms recent state-of-the-art methods across various tasks.

Moreover, our findings are backed by theoretical guarantees. We establish theoretical guarantees for the proposed MI-Min and CE-Max processes in enhancing both OoD generalization and OoD detection, as formalized in Theorem 1 and Theorem 2. Furthermore, compared to SCONE [4], InfoBound effectively mitigates the trade-off between the two tasks. We provide a detailed analysis of the under-

lying reason behind SCONE’s trade-off in Proposition 1 and explain why InfoBound alleviates this issue in Theorem 3.

## 2 RELATED WORKS

**Out-of-Distribution Generalization** aims to generalize to covariate-shifted data from the target domain. Typically, they can be categorized into three types: 1) Invariant learning-based methods [10], [11], [12], [13], [14], which involve learning data representations that remain invariant across various environments. For instance, Invariant Risk Minimization (IRM [14]) seeks to acquire data representations that align with all training distributions. Invariant representation learning techniques [10], [11], [12], [13] are designed to construct latent features impervious to non-causal data variations that do not influence final predictions. 2) Domain generalization methods aim to train models using data from one or multiple related but distinct source domains to ensure robust generalization to any OoD test domain. Some popular domain generalization techniques include Adversarial training [15], [16], Gradient-based methods [17], [18], [19], [20], Meta-learning [21], [22], [23], and Transfer learning [24], [25]. For more detailed information, we refer readers to this survey [26]. 3) Stable learning methods, which are proposed to improve the robustness and stability of machine learning models. Common techniques include data augmentation [27], ensemble methods [28], and Bayesian methods [29], etc. While these methods have exhibited varying degrees of improvement in OoD generalization performance, recent findings indicate their challenge in outperforming the standard Empirical Risk Minimization (ERM) method, especially on the covariate shift datasets [30], [31]. While these methods [32], [33], [34], [13], [18], [35], [36], [37] have exhibited varying degrees of improvement in OoD generalization performance, they focus solely on known classes, leave OoD detection without being taken into consideration, or lack theoretical underpinnings [38], [39].

Furthermore, there have been several studies applying information theory in the field of out-of-distribution (OoD) generalization. For instance, Nadjahi et al. [40] focused on efficiently evaluating mutual information within low-dimensional subspaces to bound the generalization error. Additionally, Cha et al. [35] proposed to optimize mutual information using an oracle pre-trained model, establishing a robust baseline for comparison. On the other hand, Nguyen et al. [41] utilized conditional entropy minimization to learn invariant features across domains. Unlike previous approaches that individually address mutual information or conditional entropy for OoD generalization, our method considers optimizing mutual information and conditional entropy together, which is derived by treating OoD generalization and OoD detection as two sides of one coin.

**Out-of-Distribution Detection** is the task of identifying whether a given sample belongs to ID categories. It has been a popular research topic in recent years, especially in the field of machine learning models deployed in the open world. Various methods have been proposed to tackle this challenge, methods can be categorized into two main groups: post hoc methods [42], [8], [43], [44], [45], [46], [47] and training-time regularization [48], [4], [49], [50],

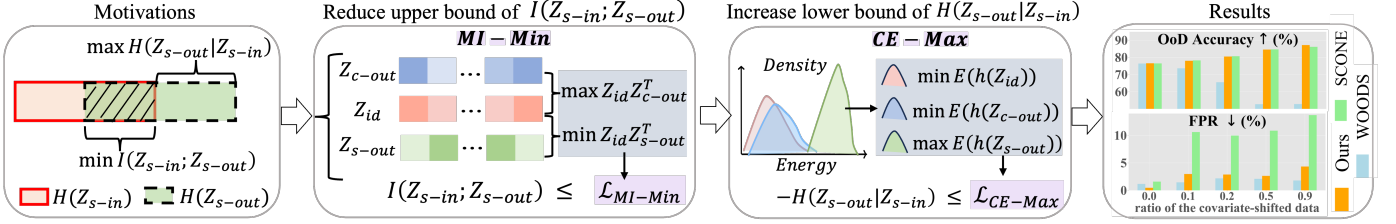


Fig. 2: The proposed InfoBound framework is grounded in information theory. To effectively separate the semantic-shifted representation  $Z_{s-out}$  from the semantic-in representation  $Z_{s-in}$  and enhance their identification, it is encouraged to simultaneously minimize their mutual information (MI)  $I(Z_{s-in}; Z_{s-out})$  and maximize the conditional entropy (CE)  $H(h(Z_{s-out})|h(Z_{s-in}))$ . To tackle the minimization of  $I(Z_{s-in}; Z_{s-out})$ , we propose the MI-Min process. It utilizes the bound-inspired loss  $\mathcal{L}_{MI-Min}$  (defined in Equation 5) to manipulate representations' distribution, effectively compressing  $I(Z_{s-in}; Z_{s-out})$  by reducing its upper bound. Furthermore, we introduce the CE-Max process, which employs an energy-based loss  $\mathcal{L}_{CE-Max}$  (defined in Equation 7) to help increase  $H(h(Z_{s-out})|h(Z_{s-in}))$ . By integrating the two novel processes, InfoBound effectively suppresses trade-offs between both tasks, yielding better overall performance as shown in Table 2.

[51], [52]. Post hoc methods typically design novel OoD score functions without altering the DNN training process. On the other hand, regularization-based methods aim to rectify the training process, compelling models to provide predictions with lower confidence. However, these methods are primarily designed for clean semantic-shifted OoD data. In real-world scenarios, a more practical case is that we only have access to a diverse mixture of data comprising various types of distribution shifts. Most previous studies primarily focus on investigating the detection ability on semantic shifts, overlooking their performance in identifying other types of OoD data. A recent work, SCONE [4], addresses this gap by exploring the use of wild mixture data, including in-distribution, covariate-shifted, and semantic-shifted data. It provides an integrated framework for both OoD generalization and OoD detection, which presents additional challenges previously unexplored [9].

### 3 METHODOLOGY

For clarity, we first explain the import notations and model assumptions before elaborating on our InfoBound as shown in Notation 1 and Assumption 1.

**Notation 1.** Given the labeled ID training data  $(X_{id}, Y)$  sampling from the ID distribution  $\mathcal{D}_{id}$ , the freely available unlabeled covariate-shifted OoD data  $X_{c-out}$  from distribution  $\mathcal{D}_{c-out}$ , and unlabeled semantic-shifted OoD data  $X_{s-out}$  from distribution  $\mathcal{D}_{s-out}$ , we denote the corresponding latent features extracted from inputs as  $Z_{id} \in \mathbb{R}^{1 \times D}$ ,  $Z_{c-out} \in \mathbb{R}^{1 \times D}$ , and  $Z_{s-out} \in \mathbb{R}^{1 \times D}$ , respectively. Let  $h$  denote the final classifier head, and  $h(Z)$  represent the classification result for representation  $Z$ . Based on information theory, the proposed InfoBound method manipulates the distribution of representations  $Z = \{Z_{id}, Z_{c-out}, Z_{s-out}\}$ .

**Assumption 1.** In practice, we assume access to labeled ID samples  $(X_{id}^i, Y^i)$ ,  $(i \in \{1, 2, \dots, n_1\})$  and unlabeled OoD samples  $X_{c-out}^i$ ,  $(i \in \{1, 2, \dots, n_2\})$  and  $X_{s-out}^i$ ,  $(i \in \{1, 2, \dots, n_3\})$ . The freely available unlabeled covariate-shifted OoD data shares the same distribution as the test covariate-shifted OoD data. We assume that ID data and covariate-shifted OoD data share the common semantic information  $Z_{s-in} \in \mathbb{R}^{1 \times D}$  (called semantic IN), while the semantic-shifted data are present as unseen classes that possess the generic semantic information  $Z_{s-out} \in \mathbb{R}^{1 \times D}$

(called semantic OUT). We suppose that the classifier  $h$  is  $L$ -Lipschitz. For the binary classification of semantic IN and OUT, no distinction is made between different categories within the same semantic label.

**Remark 1.** Having access to the unlabeled OoD data  $X_{c-out}$  and  $X_{s-out}$ , our initial step involves generating pseudo labels for them, and then we try to boost OoD generalization and OoD detection utilizing information in these samples. Without introducing any ambiguity, we still denote representations derived from the identified covariate-shifted sample and semantic-shifted sample as  $Z_{c-out}$  and  $Z_{s-out}$ , respectively. The pseudo-label generator is detailed in Section 3.3. In this paper, we first present the motivation behind our method, along with its formulation expressed in expectation form, where we omit index  $i$  in the notation. We then introduce the practical loss function used during training.

In Section 3.1, we first delve into the motivation of the proposed InfoBound and establish theoretical bounds for both mutual information and conditional entropy. Building upon bound optimization, we introduce two processes within the proposed InfoBound, namely Mutual Information Minimization (MI-Min) and Conditional Entropy Maximization (CE-Max). By optimizing these theoretical bounds, InfoBound effectively minimizes the shared information between semantic factors and thus promotes their separation. In Figure 2, we outline the motivation behind our InfoBound and intuitively illustrate the MI-Min and CE-Max processes. Next, in Section 3.2, we provide comprehensive theoretical justification for InfoBound, demonstrating its superiority in improving both OoD generalization and OoD detection and mitigating the trade-off between both tasks. Proofs for the following propositions and theorems are detailed in the Appendix. Moreover, in Section 3.3, we provide the complete algorithm of our approach, illustrating the specific method when incorporating InfoBound into different computer visual tasks.

#### 3.1 Motivations

Our proposed InfoBound is grounded in information theory. The mutual information between the semantic-shifted representation  $Z_{s-out}$  and the semantic-in representation  $Z_{s-in}$ , denoted as  $I(Z_{s-in}; Z_{s-out})$ , quantifies the amount of

shared information between them. To separate  $Z_{s-out}$  and  $Z_{s-in}$ , we can reduce their shared information by minimizing  $I(Z_{s-in}; Z_{s-out})$ . Furthermore, to enhance the recognition of semantic-out samples, it is generally desirable for the classifier to accurately predict semantic-in samples while avoiding the misclassification of semantic-out samples into any known class [8]. This requirement underscores the importance of maximizing the uncertainty in predictions for semantic-out samples, denoted as  $h(Z_{s-out})$ . In this study, we quantify this uncertainty using the conditional entropy  $H(h(Z_{s-out})|h(Z_{s-in}))$ , which measures the additional information required to determine the outcome of  $h(Z_{s-out})$  given the predictions for semantic-in samples ( $h(Z_{s-in})$ ).

### 3.1.1 Minimizing Mutual Information

As analyzed above, the goal of the Mutual Information Minimization process (MI-Min) is to distinguish between semantic IN and semantic OUT by minimizing their mutual information, i.e.,  $I(Z_{s-in}; Z_{s-out})$ . Meanwhile, this process also aims to mitigate the influence of covariate shifts, thereby improving the precision of semantic-in samples identification. In this paper, we follow previous works [53], [54], [55] to formulate  $I(Z_{s-in}; Z_{s-out})$ . Specifically, after applying softmax to the latent feature vector  $Z$ , each element in  $Z$  can be interpreted as the probability of belonging to a particular "class". The total number of "classes" is denoted as  $D$ , which corresponds to the dimension of vector  $Z$ . Consequently, the joint probability distribution  $P(Z_{s-in}, Z_{s-out})$  ( $P$  for short) can be represented by the two-dimensional matrix:  $Z_{s-in}^T Z_{s-out}$ . For symmetry about  $Z_{s-in}$  and  $Z_{s-out}$ , we further use  $(P + P^T)/2$ . Thus, we can formulate  $I(Z_{s-in}; Z_{s-out})$  as below:

$$I(Z_{s-in}; Z_{s-out}) = \sum_{d=1}^D \sum_{d'=1}^D P_{dd'} \ln \frac{P_{dd'}}{P_d \cdot P_{d'}} \quad (1)$$

where  $P_{dd'}$  is the element located at the  $d$ -th row and the  $d'$ -th column in  $(P + P^T)/2$ ;  $P_d$  and  $P_{d'}$  denote the marginal probability distributions, which can be obtained by summing over the  $d$ -th row or the  $d'$ -th column of the joint probability distribution matrix of  $(P + P^T)/2$ , respectively.

Based on the formulation in Equation 1, now we can drive the upper bound of  $I(Z_{s-in}; Z_{s-out})$  as follows:

**Lemma 1.** *The mutual information  $I(Z_{s-in}; Z_{s-out})$  is upper bounded by:*

$$\begin{aligned} I(Z_{s-in}; Z_{s-out}) &= \sum_{d=1}^D \sum_{d'=1}^D P_{dd'} \ln \frac{P_{dd'}}{P_d \cdot P_{d'}} \\ &\leq Z_{s-in} Z_{s-out}^T + \sum_{d=1}^D \sum_{d'=1}^D P_{dd'} I\{d \neq d'\} \end{aligned} \quad (2)$$

Building upon the theoretical bound in Lemma 1, our primary objective is to minimize  $Z_{s-in} Z_{s-out}^T$  in Equation 2, which helps to compress  $I(Z_{s-in}; Z_{s-out})$ . Assuming that the ID data and covariate-shifted OoD data share common semantic information, we draw inspiration from contrastive learning methods that perform pairwise comparisons between representations [56], [57], [58], [59], we estimate  $Z_{s-in}$  by solving  $\operatorname{argmin}_{Z_{id}} \mathbb{E}[\log(\exp(Z_{id} Z_{s-out}^T) / \exp(Z_{id} Z_{c-out}^T))]$ .

This estimation enables us to construct the optimization objective for the MI-Min process as:

$$\begin{aligned} \min \mathbb{E}[Z_{s-in} Z_{s-out}^T] &\implies \min \mathbb{E}[(Z_{id} Z_{s-out}^T)] \\ \text{s.t. } \mathbb{E} \left[ \log \frac{\exp(Z_{id} Z_{s-out}^T)}{\exp(Z_{id} Z_{c-out}^T)} \right] &= \min \mathbb{E} \left[ \log \frac{\exp(Z_{id} Z_{s-out}^T)}{\exp(Z_{id} Z_{c-out}^T)} \right] \end{aligned} \quad (3)$$

According to the Lagrange Multiplier method, we define the final optimization objective of the MI-Min process as below:

By Lagrange Multiplier, with the Lagrange multiplier denoted as  $\alpha$ , ( $\alpha > 0$ ), the optimization objective of  $\min I(Z_{s-in}; Z_{s-out})$  is formalized as:

$$\mathcal{L} = (1 + \alpha) \mathbb{E}[Z_{id} Z_{s-out}^T] - \alpha \mathbb{E}[Z_{id} Z_{c-out}^T] \quad (4)$$

In practice, we denote the sample size of the ID data, covariate-shifted OoD data, and semantic-shifted OoD data as  $n_1$ ,  $n_2$ , and  $n_3$ , respectively. The latent features of the three types of data are denoted as  $Z_{id}^i$ , ( $1 \leq i \leq n_1$ ),  $Z_{c-out}^k$ , ( $1 \leq k \leq n_2$ ), and  $Z_{s-out}^j$ , ( $1 \leq j \leq n_3$ ). Without loss of generality, we use  $\alpha = 1$ , then the optimization objective of  $\min I(Z_{s-in}; Z_{s-out})$  is represented as:

$$\begin{aligned} \mathcal{L}_{\text{MI-Min}} &= \frac{2}{n_1 n_3} \sum_{i=1}^{n_1} \sum_{j=1}^{n_3} Z_{id}^i (Z_{s-out}^j)^T \\ &\quad - \frac{1}{n_1 n_2} \sum_{i=1}^{n_1} \sum_{k=1}^{n_2} Z_{id}^i (Z_{c-out}^k)^T \end{aligned} \quad (5)$$

### 3.1.2 Maximizing Conditional Entropy

The Conditional Entropy Maximization process (CE-Max) is then introduced to enhance the detection of semantic-out samples, which is achieved by maximizing the conditional entropy  $H(h(Z_{s-out})|h(Z_{s-in}))$ . This optimization is driven by two key motivations: 1) The primary objective of the classifier head is to accurately and confidently predict semantic-in representations. In other words, for each semantic-in sample, the classification result should ideally be deterministic. 2) However, to facilitate detecting semantic-out samples, it is expected that these samples are not classified as any known class [8]. This requirement necessitates maximizing the uncertainty of the classification results for semantic-out samples. In this paper, we quantified this uncertainty by the conditional entropy  $H(h(Z_{s-out})|h(Z_{s-in}))$ , which satisfies:

$$H(h(Z_{s-out})|h(Z_{s-in})) \geq H(h(Z_{s-out})) - H(h(Z_{s-in})) \quad (6)$$

We opt to maximize the lower bound as shown in Equation 6, helping reduce uncertainty for  $h(Z_{s-in})$  while simultaneously maximizing uncertainty for  $h(Z_{s-out})$ . Based on the relationship between entropy and energy, we construct CE-Max's optimization objective as below:

The maximization of the lower bound for  $\max H(h(Z_{s-out}))$  is equivalent to maximizing its energy, i.e.,  $\max E(h(Z_{s-out}))$ . In this context, we define  $h_i(Z)$  as the  $i$ -th element of  $h(Z)$  and  $C$  denotes the class number. Taking  $\min H(h(Z_{s-in}))$  into consideration, we use the

following energy-based loss function for the CE-Max process in practice:

$$\begin{aligned} \mathcal{L}_{\text{CE-Max}} = & \sum_{i=1}^{n_3} \frac{1/n_3}{1 + \exp(\beta \cdot E(h(Z_{s\text{-out}}^i)))} \\ & + \sum_{i=1}^{n_1+n_2} \frac{1/(n_1+n_2)}{1 + \exp(-\beta \cdot E(h(\hat{Z}_{s\text{-in}}^i)))} \end{aligned} \quad (7)$$

where  $E(h(Z)) = -\log \sum_{i=1}^C e^{h_i(Z)}$ ,  $\hat{Z}_{s\text{-in}} = \{Z_{id}, Z_{c\text{-out}}\}$ , and  $\beta > 0$  is a learnable parameter.

### 3.2 Theoretical Guarantees

In this section, we establish theoretical guarantees for the proposed processes in enhancing both OoD generalization and OoD detection, as formalized in Theorem 1 and Theorem 2. Furthermore, compared to prior work such as SCONE [4], InfoBound effectively mitigates the trade-off between these two tasks. We provide a detailed analysis of the underlying reasons behind SCONE's trade-off in Proposition 1 and explain why InfoBound alleviates this issue in Theorem 3.

**Theorem 1. [OoD Generalization Guarantee of MI-Min]** Given the ID training data  $(X_{id}, Y)$  sampling from the ID distribution  $\mathcal{D}_{id}$ , and the freely available unlabeled covariate-shifted OoD data  $X_{c\text{-out}}$  from distribution  $\mathcal{D}_{c\text{-out}}$  and unlabeled semantic-shifted OoD data  $X_{s\text{-out}}$  from distribution  $\mathcal{D}_{s\text{-out}}$ , we train the proposed InfoBound model and we denote parameters in the converged InfoBound model as  $\omega_{\text{InfoBound}}^\infty$ . Keeping the model architecture unchanged but replacing the optimization objective with empirical risk minimization (ERM), we denote the model parameters of the ERM model at training step  $t$  as  $\omega_{\text{ERM}}^t$ . Thus, we denote the InfoBound model as  $f_{\text{InfoBound}}(X; \omega_{\text{InfoBound}}^\infty)$  and denote the ERM model at training step  $t$  as  $f_{\text{ERM}}(X; \omega_{\text{ERM}}^t)$ , ( $t \in [0, +\infty)$ ). Based on the square loss function  $\ell$ , we define InfoBound's prediction errors on covariate-shifted OoD data as:

$$\begin{aligned} \mathcal{L}_{c\text{-out}}(f_{\text{InfoBound}}(\omega_{\text{InfoBound}}^\infty)) := & \\ \mathbb{E}_{(X,Y) \in \mathcal{D}_{c\text{-out}}} [\ell(f_{\text{InfoBound}}(X; \omega_{\text{InfoBound}}^\infty), Y)], \end{aligned} \quad (8)$$

and the ERM model's prediction errors as:

$$\mathcal{L}_{c\text{-out}}(f_{\text{ERM}}(\omega_{\text{ERM}}^t)) := \mathbb{E}_{(X,Y) \in \mathcal{D}_{c\text{-out}}} [\ell(f_{\text{ERM}}(X; \omega_{\text{ERM}}^t), Y)].$$

Then for  $\forall \delta > 0$  and  $\forall t > 0$ , the prediction errors of InfoBound and ERM satisfy:

$$\mathbb{P} \left( \frac{\mathcal{L}_{c\text{-out}}(f_{\text{InfoBound}}(\omega_{\text{InfoBound}}^\infty))}{\min_{t>0} \mathcal{L}_{c\text{-out}}(f_{\text{ERM}}(\omega_{\text{ERM}}^t))} \geq \delta \right) = 0 \quad (9)$$

From Theorem 1, InfoBound's prediction errors on covariate-shifted OoD data, i.e.,  $\mathcal{L}_{c\text{-out}}(f_{\text{InfoBound}}(\omega_{\text{InfoBound}}^\infty))$ , are consistently lower than those of ERM, i.e.,  $\mathcal{L}_{c\text{-out}}(f_{\text{ERM}}(\omega_{\text{ERM}}^t))$ , at any training time  $t$ . This provides a theoretical guarantee that the proposed InfoBound method enhances OoD generalization compared to the vanilla ERM approach.

**Theorem 2. [OoD Detection Guarantee by the Synergistic Effect of MI-Min and CE-Max]** Suppose that the classifier  $h$  is  $L$ -Lipschitz. Under the loss function defined in Equation 5

and Equation 7, the training process of InfoBound satisfies the conditions of  $\mathcal{L}_{\text{MI-Min}} \leq \varepsilon_m$  and  $\mathcal{L}_{\text{CE-Max}} \leq \varepsilon_c$  after training. We consider a binary classification task distinguishing between semantic IN and semantic OUT, where the classification boundary is defined by  $E(h(Z)) = 0$  and  $E(h(Z))$  is the energy score of  $h(Z)$ . If  $\varepsilon_c \leq (1 + e^{2\beta L \sqrt{2 - |\varepsilon_m|}})^{-1}$ , then any ID sample satisfying  $E(h(Z_{id})) \leq -\frac{1}{\beta} \log(\frac{1}{\varepsilon_c} - 1)$ , will have its covariate-shifted OoD counterpart detected as semantic IN. Meanwhile, the mean energy score of semantic-shifted OoD samples is lower-bounded by  $\mathbb{E}_{Z_{s\text{-out}}} [E(h(Z_{s\text{-out}}))] \geq 2L \sqrt{2 - |\varepsilon_m|}$ .

Under mild conditions on the training state of MI-Min and CE-Max, Theorem 2 provides a certifiable guarantee for detecting covariate-shifted OoD samples as semantic IN. Additionally, not only can the MI-Min process enhance OoD generalization as demonstrated in Theorem 1, but also it can raise the lower bound on the energy scores of semantic-shifted OoD samples, i.e.,  $\mathbb{E}_{Z_{s\text{-out}}} [E(h(Z_{s\text{-out}}))] \geq 2L \sqrt{2 - |\varepsilon_m|}$ , which enhances the discrimination between covariate-shifted and semantic-shifted OoD data.

**Proposition 1. [SCONE's Margin Leads to Trade-offs between OoD Generalization and OoD Detection]** Suppose there exist covariate-shifted and semantic-shifted data satisfying  $\|Z_{id} - Z_{c\text{-out}}\|_2 \leq \varepsilon_0$  and  $\|Z_{id} - Z_{s\text{-out}}\|_2 \leq \varepsilon_0$ . Assume that the classifier  $h$  is  $L$ -Lipschitz. We consider a binary classification task distinguishing between semantic IN and semantic OUT, where the classification boundary is defined by  $E(h(Z)) = 0$  and  $E(h(Z))$  is the energy of  $h(Z)$ . In the SCONE method, a margin  $\eta$  is incorporated on ID data. While setting  $\eta \leq -L\varepsilon_0$  allows covariate-shifted OoD points to be detected as semantic IN and increases the logit for their correct classes, it simultaneously results in all semantic-shifted samples satisfying  $\|Z_{id} - Z_{s\text{-out}}\|_2 \leq \varepsilon_0$  to be incorrectly detected as semantic IN.

Proposition 1 provides theoretical insights into SCONE's trade-offs between OoD generalization and OoD detection. It suggests that incorporating a margin on ID data causes covariate-shifted samples, which satisfy  $\|Z_{id} - Z_{c\text{-out}}\|_2 \leq \varepsilon_0$ , to be correctly detected as semantic IN. Simultaneously, this increases the logit for their correct classes, thereby enhancing OoD generalization. However, it also comes at the cost of incorrectly detecting all semantic-shifted samples, which satisfy  $\|Z_{id} - Z_{s\text{-out}}\|_2 \leq \varepsilon_0$ , as semantic IN.

**Theorem 3. [InfoBound Achieves Lower False Positive Rate (FPR) than SCONE]** Suppose there exist covariate-shifted and semantic-shifted samples such that their embeddings satisfy  $\|Z_{id} - Z_{c\text{-out}}\|_2 \leq \varepsilon_0$  and  $\|Z_{id} - Z_{s\text{-out}}\|_2 \leq \varepsilon_0$ . Based on the energy score, we assume there exists a threshold  $\theta_0$  that can detect all the covariate-shifted OoD samples as semantic IN while correctly identifying a portion of the semantic-shifted OoD samples as semantic OUT. If InfoBound satisfies the condition of  $\mathcal{L}_{\text{CE-Max}} \leq \varepsilon_c$  after training, then the false positive rate (FPR) of InfoBound on the semantic-shifted data, denoted as  $\text{FPR}_{\text{InfoBound}}(Z_{s\text{-out}})$ , is lower than that of SCONE, denoted as  $\text{FPR}_{\text{SCONE}}(Z_{s\text{-out}})$ . That is,  $\text{FPR}_{\text{InfoBound}}(Z_{s\text{-out}}) < \text{FPR}_{\text{SCONE}}(Z_{s\text{-out}})$ .

Theorem 3 states that under the condition that all covariate-shifted OoD samples are detected as semantic IN, the SCONE method also classifies semantic-shifted OoD

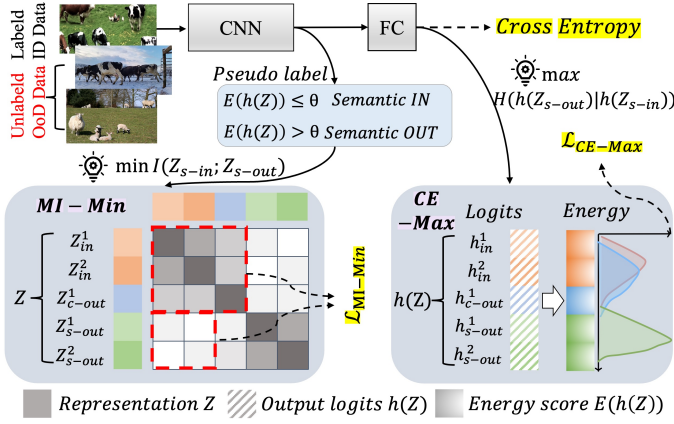


Fig. 3: Pipeline of the proposed InfoBound for image classification. We employ an energy-based pseudo-label generator to select semantic-out samples ( $E(h(Z)) > \theta$ ) and semantic-in samples ( $E(h(Z)) \leq \theta$ ). The threshold  $\theta$  is a hyperparameter that can be set referring to the energy score of ID training data. We detail the hyperparameter setting in the experiment section. Pre-trained models are utilized to ensure the quality of pseudo labels.

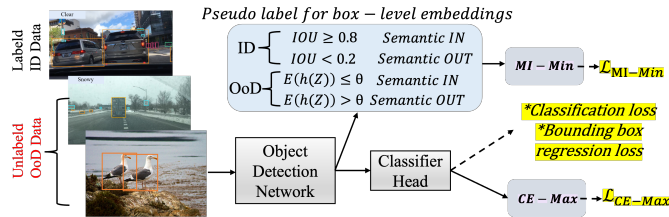


Fig. 4: Pipeline of the proposed InfoBound for object detection. For ID samples, we only select clean proposals ( $\text{IoU} \geq 0.8$ ), ensuring the quality of box-level embeddings from ID data. The threshold  $\theta$  is a hyperparameter that we detail in the experiment section.

samples—whose nearest distance to the ID data is no larger than that of covariate-shifted OoD—as semantic IN. In contrast, our method more effectively distinguishes between semantic-shifted OoD and covariate-shifted OoD samples with the same nearest distance, resulting in a lower False Positive Rate (FPR) compared to SCONE.

### 3.3 Algorithm

Combining the proposed loss functions with the original loss  $\mathcal{L}_0$  (e.g., the Cross-Entropy loss for classification), the final optimization objective of the proposed InfoBound is introduced as:

$$\mathcal{L}_{\text{InfoBound}} = \mathcal{L}_0 + \lambda(\mathcal{L}_{\text{MI-Min}} + \mathcal{L}_{\text{CE-Max}}) \quad (10)$$

where  $\lambda$  is the hyperparameter that can be chosen based on the validation procedure. In this section, we provide details of our algorithm for image classification and object detection. See Figure 3 and Figure 4 for the overview of our InfoBound in the two practical tasks.

**InfoBound for Image Classification** Leveraging the freely available unlabeled data that captures both covariate shifts and semantic shifts, our initial step involves generating

pseudo labels for these unlabeled data. This enables us to preliminarily screen samples and distinguish between those belonging to the semantic-shifted OoD data and those that do not. In the pseudo-label generator, we utilize energy scores to estimate the degree of out-of-distribution (OoD) characteristics of a sample, where a higher energy score indicates a greater likelihood of being OoD. Specifically, for each representation  $Z$ , based on its classification result  $h(Z)$ , we calculate its energy score, denoted as  $E(h(Z))$ . By employing a pre-determined threshold, denoted as  $\theta$ , we classify the representation  $Z$  as either semantic OUT when  $E(h(Z)) > \theta$ , or semantic IN when  $E(h(Z)) \leq \theta$ . The threshold  $\theta$  is a hyperparameter that can be set based on the energy scores of ID data. Subsequently, we employ the final objective function  $\mathcal{L}_{\text{InfoBound}}$  during training to effectively address both covariate and semantic shifts. Specifically, as shown in Equation 5, we minimize the inner product between the embeddings of labeled ID data and identified semantic-out data, while encouraging alignment between the embeddings of ID data and identified semantic-in data. In addition, as shown in Equation 7, we maximize (or minimize) the energy score for identified semantic-out (or ID and identified semantic-in) data to increase the conditional entropy, improving the model’s ability to distinguish between semantic-in and semantic-out samples. As demonstrated in Theorem 1-2, benefiting from the synergistic effect between the MI-Min and CE-Max processes, the InfoBound method can improve both the OoD detection and OoD generalization tasks.

**InfoBound for Object Detection** In the context of object detection, we also utilize energy scores to select the semantic-in objects and the semantic-out objects from the bounding box proposals of unlabeled data. To ensure the quality of box-level embeddings for ID data, we discard any bounding box proposals generated by the detection backbone that have a low Intersection over Union (IoU) with the ground-truth objects. Specifically, we retain only the clean proposals with a high IoU (i.e.,  $\text{IoU} \geq 0.8$ ), thereby ensuring the reliability of the box-level ID embeddings. In addition to the bounding box regression loss and classification loss, the proposed regularization terms  $\mathcal{L}_{\text{MI-Min}}$  and  $\mathcal{L}_{\text{CE-Max}}$  are introduced. These regularization terms are implemented similarly to how they are applied in image classification. All operations, including representation manipulation in MI-Min and energy-based regularization in CE-Max, are performed on the box-level embeddings and box-level logits, respectively. Specifically, we first generate pseudo labels for the proposals of the unlabeled wild data. After that, as shown in Equation 5, we minimize the inner product between the box-level embedding of the ID objects and the box-level embedding of the identified semantic-out objects. Simultaneously, we enforce alignment between the box-level embedding of the ID objects and the box-level embedding of the identified semantic-in objects. Furthermore, as shown in Equation 7, we maximize (or minimize) the energy scores corresponding to semantic-out (or semantic-in) proposals to increase the conditional entropy of the identified semantic-out data, thereby enhancing the separability between different semantic IN and semantic OUT.

TABLE 1: Main results: comparison with competitive OoD generalization and OoD detection methods on CIFAR-10. Our experiments show that InfoBound outperforms the state-of-the-art method SCONE in OoD detection, achieving a significant reduction of around 5.5% in FPR, while maintaining comparable OoD generalization results.

Method	SVHN, CIFAR-10-C				Texture, CIFAR-10-C				LSUN-C, CIFAR-10-C			
	OoD Acc.↑	ID Acc.↑	FPR↓	AUROC↑	OoD Acc.↑	ID Acc.↑	FPR↓	AUROC↑	OoD Acc.↑	ID Acc.↑	FPR↓	AUROC↑
<i>OoD detection</i>												
MSP	75.05	94.84	48.49	91.89	75.05	94.84	59.28	88.50	75.05	94.84	30.80	95.65
ODIN	75.05	94.84	33.35	91.96	75.05	94.84	49.12	84.97	75.05	94.84	15.52	97.04
Energy	75.05	94.84	35.59	90.96	75.05	94.84	52.79	85.22	75.05	94.84	8.26	98.35
Mahalanobis	75.05	94.84	12.89	97.62	75.05	94.84	15.00	97.33	75.05	94.84	39.22	94.15
ViM	75.05	94.84	21.95	95.48	75.05	94.84	29.35	93.70	75.05	94.84	5.90	98.82
KNN	75.05	94.84	28.92	95.71	75.05	94.84	39.50	92.73	75.05	94.84	28.08	95.33
<i>OoD generalization</i>												
ERM	75.05	94.84	35.59	90.96	75.05	94.84	52.79	85.22	75.05	94.84	8.26	98.35
Mixup	79.17	93.30	97.33	18.78	79.17	93.30	58.24	75.70	79.17	93.30	52.10	76.66
IRM	77.92	90.85	63.65	90.70	77.92	90.85	59.42	87.81	77.92	90.85	36.67	94.22
VREx	76.90	91.35	55.92	91.22	76.90	91.35	65.45	85.46	76.90	91.35	51.50	91.56
<i>Learning w. <math>\mathbb{P}_{wild}</math></i>												
OE	37.61	94.68	0.84	99.80	44.71	92.84	29.36	93.93	41.37	93.99	3.07	99.26
Energy (w. outlier)	20.74	90.22	0.86	99.81	49.34	94.68	16.42	96.46	32.55	92.97	2.33	99.93
WOODS	52.76	94.86	2.11	99.52	83.14	94.49	39.10	90.45	76.90	95.02	1.80	99.56
SCONE	84.69	94.65	10.86	97.84	85.56	93.97	37.15	90.91	84.58	93.73	10.23	98.02
InfoBound (ours)	84.38	94.70	2.92	99.45	85.07	94.73	35.22	90.96	84.63	94.60	3.72	99.12
	±0.63	±0.05	±1.05	±0.24	±0.23	±0.07	±0.79	±0.27	±0.13	±0.10	±0.91	±0.24

TABLE 2: Comprehensive evaluations on OoD detection and generalization. InfoBound effectively incorporates more semantic-in samples into the classification process, achieving significant improvements in classification accuracy for both ID data and covariate-shifted data. Ablation studies for threshold  $\tau$  are provided in Appendix C to demonstrate InfoBound’s robustness on both tasks.

Method	SVHN, CIFAR-10-C			Texture, CIFAR-10-C			LSUN-C, CIFAR-10-C		
	OoD SI-Acc.↑	ID SI-Acc.↑	SI-Recall↑	OoD SI-Acc.↑	ID SI-Acc.↑	SI-Recall↑	OoD SI-Acc.↑	ID SI-Acc.↑	SI-Recall↑
<i>Learning w. <math>\mathbb{P}_{wild}</math></i>									
SCONE	58.99	85.50	62.13	63.56	86.05	67.30	61.40	85.95	64.92
InfoBound (ours)	76.82	86.55	85.95	69.55	86.56	74.07	78.30	86.92	87.78

## 4 EXPERIMENTS

### 4.1 Experiments for Image Classification

**Datasets** Following the common benchmark in the literature [4], we use CIFAR-10 [60] as the ID data. For the covariate-shifted data, we use CIFAR-10-C [61] with Gaussian additive noise for our main experiments, and provide ablations on other types of covariate shifts in Appendix A. For semantic shifted OoD data, we use three natural image datasets: SVHN [62], Textures [63], and LSUN-Crop [64]. Following SCONE, we denote the distribution of the wild mixture as  $\mathbb{P}_{wild} = (1 - \pi_c - \pi_s)\mathbb{P}_{in} + \pi_c\mathbb{P}_{out}^{covariate} + \pi_s\mathbb{P}_{out}^{semantic}$ , where  $\pi_c$  and  $\pi_s$  are the proportion of covariate-shifted (semantic IN) data and semantic-shifted (semantic OUT) data, respectively;  $\mathbb{P}_{in}$ ,  $\mathbb{P}_{out}^{covariate}$ , and  $\mathbb{P}_{out}^{semantic}$  denote the distribution of ID data, covariate-shifted data, and semantic-shifted data, respectively.

**Comprehensive Evaluations** Following the standard metrics used in previous works [4], [8], [9], we evaluate model performance from three perspectives: 1) In-distribution performance: the classification accuracy on the ID test sets (**ID Acc**); 2) OoD generalization: the classification accuracy on the covariate-shifted test sets (**OoD Acc**); 3) OoD detection: the false positive rate of semantic-shifted samples when the true positive rate of ID samples is 95% (**FPR95**, the lower the better); the area under the receiver operating characteristic curve (**AUROC**, the higher the better).

In practical scenarios where the ground truth of semantic information is unavailable for the wild mixture, a common approach is to first determine the semantic labels of these test samples. In this paper, we propose comprehensive metrics to address these challenges. Based on energy scores obtained from the validation set, a threshold is selected to

identify semantic-in and semantic-out samples. Test samples with energy scores above the threshold are considered to be semantic OUT, while samples with lower energy scores are identified as semantic IN. Next, only the identified semantic-in samples are classified, and the classification accuracy on these samples is calculated as Semantic In Accuracy (**SI-Acc**). SI-Acc is determined by dividing the number of correctly classified semantic-in samples by the total number of semantic-in samples. Mathematically, we propose the following metrics:

$$\text{ID SI-Acc} : \mathbb{E}_{(x,y) \sim \mathbb{P}_{in}} (\mathbb{1}\{E(h(Z)) \leq \tau \wedge \hat{y}(h(Z)) = y\}) \quad (11)$$

$$\text{OoD SI-Acc} : \mathbb{E}_{(x,y) \sim \mathbb{P}_{out}^{covariate}} (\mathbb{1}\{E(h(Z)) \leq \tau \wedge \hat{y}(h(Z)) = y\}) \quad (12)$$

$$\text{SI-Recall} : \mathbb{E}_{(x,y) \sim \mathbb{P}_{out}^{covariate}} (\mathbb{1}\{E(h(Z)) \leq \tau\}) \quad (13)$$

where  $\tau$  is the threshold corresponding to that 95% in-distribution validation samples are correctly identified as semantic IN;  $\hat{y}(h(Z)) := \text{argmax}_y h_y(Z)$  is the prediction label for representation  $Z$ , and  $h_y(Z)$  denotes the  $y$ -th element of the prediction  $h(Z)$ . ID SI-Acc, OoD SI-Acc, and SI-Recall reflect the final classification accuracy on ID data, classification accuracy on covariate-shifted OoD data, and the recall rate for semantic-in samples, respectively.

**Experiment Details** For fair comparisons, we adopt the same pre-trained WideResNet architecture as in [4], using identical hyperparameters for batch size, learning rate, and other optimizer configurations. During training, we implement early stopping and allow training for a maximum of 100 epochs. The additional hyperparameters introduced by InfoBound are the threshold  $\theta$  in the pseudo-label generator

TABLE 3: Ablations on mixing ratios  $\pi_c$ . We train on CIFAR-10 as ID, using CIFAR-10-C as covariate-shifted data and SVHN as semantic-shifted data (with fixed  $\pi_s = 0.1$ ). For the SCONE [4] method, we set the margin as  $-10$  following its original paper.

$\pi_c$	Method	OoD Acc.↑	ID Acc.↑	FPR↓	AUROC↑
0.0	SCONE	76.52	<b>94.93</b>	1.60	99.71
	INFOBOUND	<b>76.54</b>	94.85	<b>0.48</b>	<b>99.91</b>
0.1	SCONE	<b>78.27</b>	94.88	10.61	97.91
	INFOBOUND	78.04	<b>94.92</b>	<b>2.98</b>	<b>99.41</b>
0.2	SCONE	<b>80.70</b>	<b>94.93</b>	9.97	98.04
	INFOBOUND	80.54	94.90	<b>2.89</b>	<b>99.47</b>
0.5	SCONE	<b>84.69</b>	94.65	10.86	97.84
	INFOBOUND	84.59	<b>94.85</b>	<b>2.64</b>	<b>99.50</b>
0.9	SCONE	86.18	94.64	13.68	97.41
	INFOBOUND	<b>87.18</b>	<b>94.78</b>	<b>4.34</b>	<b>99.15</b>

TABLE 4: Ablation study results on  $\mathcal{L}_{MI-Min}$  and  $\mathcal{L}_{CE-Max}$ .

Method	OoD Acc.↑	ID Acc.↑	FPR↓	AUROC↑
w/o $\mathcal{L}_{MI-Min}, \mathcal{L}_{CE-Max}$	83.44	<b>94.79</b>	21.89	94.95
w/ $\mathcal{L}_{CE-Max}$	83.54	94.75	24.00	94.33
w/ $\mathcal{L}_{MI-Min}$	84.68	94.66	14.97	96.39
INFOBOUND	<b>84.69</b>	94.68	<b>13.95</b>	<b>96.51</b>

negligible performance degradation in OoD detection (approximately 5% worse than WOODS in FPR). Successfully addressing this trade-off between OoD generalization and OoD detection, InfoBound outperforms the state-of-the-art method SCONE in OoD detection, achieving a remarkable reduction of around 5.5% in FPR, while maintaining comparable OoD generalization results. Notably, we also perform a comprehensive evaluation of the two key issues based on our proposed metrics. As shown in Table 2, InfoBound effectively incorporates more semantic-in samples into the classification process, achieving significant improvements in the final classification accuracy for both ID data and covariate-shifted OoD data in real-world scenarios.

**Ablations on mixing ratios** In Table 3, we ablate the effect of mixing ratios  $\pi_c$ . It is observed that SCONE is sensitive to the ratio of covariate-shifted data. Increasing  $\pi_c$  generally improves SCONE’s OoD generalization results but at the cost of OoD detection performances. This sensitivity can be attributed to the decrease in semantic outlier information when a larger  $\pi_c$  is used. In contrast, the proposed InfoBound achieves superior OoD generalization results while also demonstrating robustness in OoD detection, even at high  $\pi_c$  values such as 0.9.

**Ablations on MI-Min and CE-Max** We ablate on the proposed MI-Min and CE-Max processes to check each component’s role. The corresponding experiment results are presented in Table 4, highlighting some noteworthy observations: 1) When implementing only  $\mathcal{L}_{MI-Min}$ , we obtained improvements both in OoD generalization and OoD detection capabilities. This indicates that the MI-Min process plays a crucial role in enhancing the model’s ability to handle different distribution shifts. 2) However, only implementing  $\mathcal{L}_{CE-Max}$  alone seemed to have a counterproductive effect, potentially hindering OoD detection. This underscores the importance of the MI-Min process in manipulating the embedding space of various types of datasets. 3) Once the high-quality embeddings are established, which can be achieved by incorporating  $\mathcal{L}_{MI-Min}$ , the subsequent introduction of  $\mathcal{L}_{CE-Max}$  can further enhance OoD detection without compromising OoD generalization. Moreover, we perform ablation studies on the coefficient of InfoBound loss. As shown in Figure 5a, the higher OoD accuracies concentrated on the areas with a larger coefficient of the proposed  $\mathcal{L}_{MI-Min} + \mathcal{L}_{CE-Max}$ , which demonstrates the efficacy of our MI-Min and CE-Max processes, allowing our learned representations to better capture semantic IN and thus facilitating OoD generalization. Figure 5a-5b also suggests the appropriate range of  $\theta$  to ensure the high quality of pseudo labels.

**Visualization of Energy Score Distributions** In Figure 6, we visualize the energy score distributions for both our method and SCONE. The visualization highlights the following observations: (1) the energy score distributions of

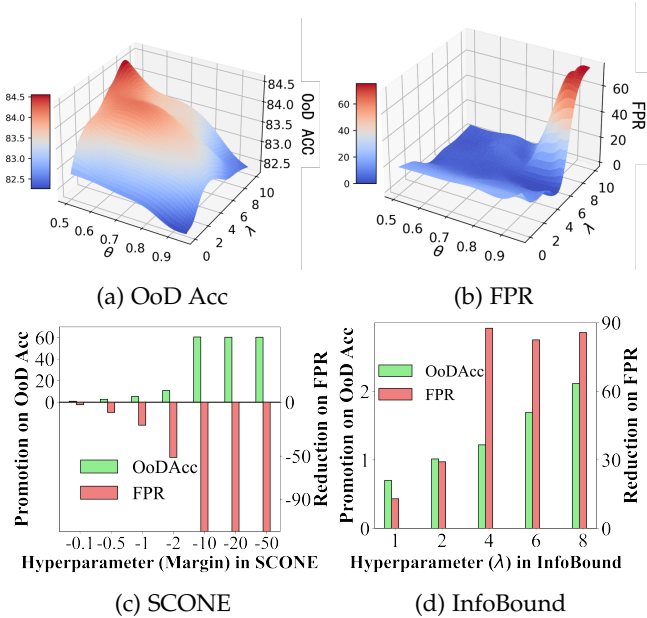


Fig. 5: (a)-(b): The sensitivity of InfoBound to hyperparameters  $\theta$  and  $\lambda$ . ( $\theta$ : threshold in pseudo-label generator;  $\lambda$ : the coefficient of  $\mathcal{L}_{MI-Min} + \mathcal{L}_{CE-Max}$ ). (c)-(d): Relative improvements on both tasks compared to the vanilla model. SCONE exhibits significant performance degradation in OoD detection. InfoBound enhances both tasks benefiting from the synergistic effect between MI-Min and CE-Max.

and the coefficient  $\lambda$  of the regularization terms in Equation 10. We search for their optimal values by maximizing the ID Acc on validation sets. Specifically, we search for  $\theta$  in the range of  $[0.5, 0.6, \dots, 1.0]$  and  $\lambda$  in the range of  $[1, 2, \dots, 10]$ .

**Experiment Results** We present the main results in Table 1, where InfoBound establishes the overall best performance in both OoD generalization and OoD detection. When compared to competitive approaches that focus on either OoD generalization or OoD detection, such as IRM, VREx, KNN, and Energy, InfoBound surpasses them by a significant margin. When considering methods that leverage additional wild data, the most recent approach SCONE achieves strong OoD generalization results but shows a non-



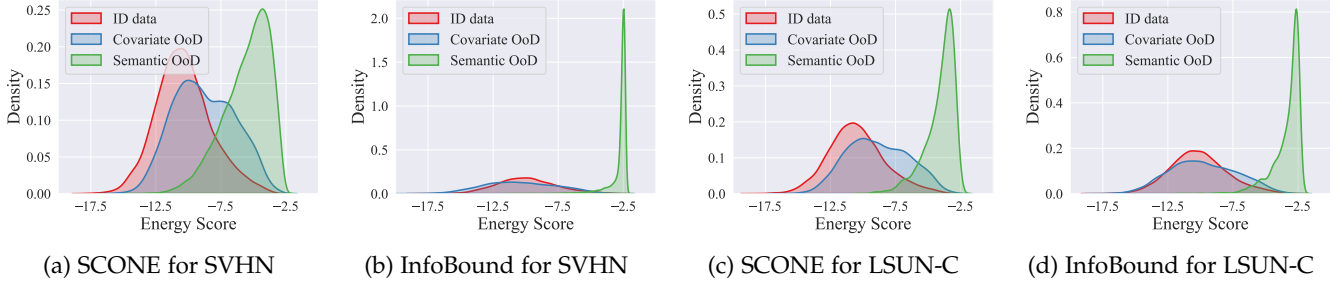


Fig. 6: Qualitative analysis of energy score visualization between InfoBound and SCONe on semantic-shifted OoD datasets (SVHN and LSUN-C), using the same covariate-shifted OoD dataset (CIFAR-10-C), and the ID dataset (CIFAR-10). With our InfoBound framework, we observed that the energy score distribution of CIFAR-10 and CIFAR-10-C exhibit better alignment. In contrast, the energy score distribution of CIFAR-10 and semantically-shifted OoD data demonstrate greater differences. This observation suggests that our approach leads to improved OoD detection performance.

TABLE 5: ImageNet benchmark: we use ImageNet-100 as ID, ImageNet-100-C for  $\mathbb{P}_{\text{ood}}^{\text{covariate}}$  and iNaturalist for  $\mathbb{P}_{\text{ood}}^{\text{semantic}}$ .

$\mathbb{P}_{\text{ood}}^{\text{covariate}} / \mathbb{P}_{\text{ood}}^{\text{semantic}}$	Method	ID/OoD Generalization		OoD Detection	
		ID-Acc. $\uparrow$	OoD-Acc. $\uparrow$	FPR $\downarrow$	AUROC $\uparrow$
ImageNet-100-C /	MSP	89.34	84.96	41.17	93.58
	Energy	89.34	84.96	43.07	92.94
	Maxlogits	89.34	84.96	39.50	93.69
iNaturalist	WOODS	81.76	25.80	1.83	99.42
	SCONe	88.42	81.90	9.93	98.33
	<b>InfoBound</b>	89.39 $\pm 0.13$	85.00 $\pm 0.45$	5.18 $\pm 0.74$	99.07 $\pm 0.10$

ID data and covariate-shifted data exhibit a higher resemblance when using our method. This improvement also offers evidence for the effectiveness of the MI-Min process in enhancing alignment between ID samples and covariate-shifted samples. (2) the significant disparity in energy scores between covariate-shifted data and semantic-shifted data shows InfoBound’s ability to detect semantic OoD.

**Effectiveness in Mitigating Trade-offs** In Figure 5c-5d, we present visualizations of the enhanced performance achieved by InfoBound and SCONe compared to the vanilla model. For fair comparisons, the maximum value range of hyperparameters for comparison was chosen to ensure comparable performance on OoD Acc. It is observed that: 1) As we increase the “margin” value in SCONe, SCONe consistently enhances the OoD Acc. However, there is a notable trade-off as it leads to significant performance degradation in OoD detection. 2) In contrast, our InfoBound considers OoD generalization against covariate factors and OoD detection as interconnected aspects, yielding improved performance in both aspects via the synergistic effect between MI-Min and CE-Max.

**Experiments on ImageNet** In Table 5, we provide the large-scale dataset results on the ImageNet benchmark. We use ImageNet-100 as the ID data ( $\mathbb{P}_{\text{in}}$ ). For the covariate-shifted OoD data ( $\mathbb{P}_{\text{out}}^{\text{covariate}}, \pi_c = 0.5$ ), we construct ImageNet-100-C by adding Gaussian noise  $\mathcal{N}(0, 1)$  to ImageNet-100. For the semantic-shifted OoD data, we use the iNaturalist dataset [65] ( $\mathbb{P}_{\text{ood}}^{\text{semantic}}, \pi_s = 0.1$ ). We finetune ResNet-34 [66] (pre-trained on ImageNet-1K) for 10 epochs on ID data with an initial learning rate of 0.001 and a batch size of 128. The results in Table 5 indicate that our method effectively reduces the trade-off, improving both OoD classification accuracy and OoD detection compared to SCONe.

**Experiments on Large-scale Pre-trained Models** Further-

more, to evaluate the effectiveness of our InfoBound on the large-scale pre-trained model, we conduct experiments based on the widely used CLIP model (Contrastive Language-Image Pre-training, [67]). CLIP has been pre-trained on a vast collection of image-text pairs from the web, enabling it to access general knowledge for open-vocabulary classification tasks. However, optimizing open-vocabulary models for downstream tasks often involves further fine-tuning of pre-trained models. It has been pointed out that the fine-tuned model can easily overfit the training data [70], [71], thus may compromise its recognition ability for semantic OoD. In Table 6, we fine-tuned CLIP using partial (40%) classes from ImageNet-1K [72]. These 40% classes constitute in-distribution (ID) data, while the remaining classes are considered semantic-shifted OoD data. Based on energy scores, we evaluated OoD detection results for the remaining classes. We also report the OoD generalization performance on the ID classes from ImageNet-A [73], ImageNet-R [74], ImageNet-Sketch [75], and ImageNet-V2 [76]. The CLIP model obtained the FPR95 result up to 77.3%, facing challenges in detecting unseen classes. Our InfoBound method leads to around 20% improvements on FPR95, showcasing its superiority in handling semantic shifts for open vocabulary models.

We also provide comparisons between SCONe and InfoBound based on the CLIP-based experiments in Table 6. We integrate the SCONe’s loss into both CoOp and CLIP-Adapter, setting the margin  $\eta = -10$  as recommended in the original paper. Compared to the vanilla model, leveraging the SCONe method results in lower FPR95 but at the cost of reduced OoD accuracy. This may be due to SCONe’s optimization objective, which aims to classify as many samples from the wild mixture as semantic OoD. This approach can inadvertently introduce a trade-off between OoD generalization and OoD detection, as it may lead to misclassification of certain covariate-shifted samples, thereby reducing overall OoD accuracy. The proposed InfoBound method achieves around 14% improvement in FPR95, demonstrating its superiority in handling semantic shifts under the few-shot setting. Meanwhile, InfoBound also achieves the highest test accuracy on covariate-shifted OoD data, showcasing its effectiveness in enhancing both tasks simultaneously.

TABLE 6: Comparison with CLIP [67], recent fine-tuning methods (such as CoOp [68] and CLIP-Adapter [69]), and our InfoBound on the ImageNet dataset. Models are fine-tuned with 4-shot samples on ViT-B/16. We evaluate the performances of CoOp [68] and CLIP-Adapter [69]) following their original papers.

Method	CLIP	CoOp	CLIP-Adapter	CoOp +SCONE	CLIP-Adapter +SCONE	CLIP-Adapter +InfoBound
ID ACC	78.2 (0.6)	80.6 (0.5)	81.0 (0.5)	80.9 (0.4)	81.0 (0.1)	<b>81.3 (0.5)</b>
OoD ACC	58.4 (0.7)	62.5 (1.0)	62.0 (0.7)	62.0 (0.6)	61.4 (0.8)	<b>62.6 (0.3)</b>
FPR95	77.3 (3.3)	78.3 (2.1)	70.6 (3.8)	75.3 (1.5)	65.7 (8.1)	<b>51.5 (3.7)</b>

TABLE 7: Details of the proposed benchmark dataset for both OoD generalization and OoD detection in the context of object detection. Quantity denotes the number of examples available during the training phase, while GT indicates the availability of ground-truth labels during training.

Details of the Proposed Benchmark Dataset					
Distribution	Dataset	Attribute	Quantity <sup>1</sup>	Semantic Label <sup>2</sup>	GT <sup>2</sup>
In-Distribution	BDD-100K	clear and overcast	full data	IN	✓
Covariate Shifts	BDD-100K	rainy, foggy, partly cloudy, and snowy	2/5/20	IN	✗
Semantic Shifts	MS-COCO	-	2/5/20	OUT	✗
	OpenImages	-	2/5/20	OUT	✗

<sup>1</sup> There are a total of  $N$  ( $N \in \{2, 5, 20\}$ ) unlabeled images that exhibit covariate shifts and a total of  $N$  ( $N \in \{2, 5, 20\}$ ) unlabeled images that demonstrate semantic shifts during the training process.

<sup>2</sup> Semantic label for OoD data is not available during the training phase.

### 4.2 Experiments for Object Detection

To the best of our knowledge, there has not been any exploration of a unified framework for both OoD detection and OoD generalization in the context of object detection. In this section, following the existing benchmark [50], we first compare InfoBound with the most recent algorithms in the context of OoD object detection. Furthermore, we introduce two standard datasets comprising the two types of distribution shifts, serving as benchmarks for investigating both OoD generalization and OoD detection for object detection.

**Benchmark Datasets for OoD Detection** Following [51], we use PASCAL-VOC [77] and Berkeley DeepDrive (BDD100K, [78]) as the ID training data. PASCAL-VOC consists of the following 20 labels: Person, Car, Bicycle, Boat, Bus, Motorbike, Train, Airplane, Chair, Bottle, Dining Table, Potted Plant, TV, Sofa, Bird, Cat, Cow, Dog, Horse, and Sheep. BDD-100k consists of these 10 labels: Pedestrian, Rider, Car, Truck, Bus, Train, Motorcycle, Bicycle, Traffic light, and Traffic sign. For both tasks, we evaluate on two OoD datasets that contain a subset (validation set) of images from MS-COCO [79] and OpenImages [80]. All overlapping classes are removed from the OoD datasets and there is no any class redundancy or hierarchical inclusion (e.g., bird and magpie) between the ID training samples and OoD samples.

**Benchmark Datasets for Both OoD Generalization and OoD Detection** In this paper, we introduce the standard dataset comprising both covariate shifts and semantic shifts, serving as benchmarks for investigating both OoD generalization and OoD detection in the context of object detection. Now we detail our constructed dataset as follows:

The large-scale automatic driving dataset, BDD100K [78], is considered to evaluate OoD generalization perfor-

mances. BDD100K contains 80,000 labeled images with 10 annotated object categories, including Pedestrian, Rider, Car, Truck, Bus, Train, Motorcycle, Bicycle, Traffic light, and Traffic sign. Each image has three attribute labels which indicate the condition, including the weather, scene and time for data collection and we remove the images with an undefined attribute label. Following the previous study of DetectBench [81], we construct OoD environments using the attribute weather labels. Specifically, the ID training examples are sampled with attribute weather labels including “clear” and “overcast”, while the covariate-shifted data is constructed with examples under “rainy”, “foggy”, “partly cloudy”, and “snowy”. For semantic-out data, we use the subset of validation sets from MS-COCO [79] and OpenImages [80] as with the previous studies [51], [82], [50]. It should be emphasized that we typically rely on labeled ID data for the supervised learning of classification and localization. Meanwhile, we have access to the unlabeled OoD datasets comprising of both covariate shifts and semantic shifts. In the proposed InfoBound method, the unlabeled OoD data is leveraged to reshape the embedding space of ID training data by the InfoBound loss. Therefore, utilizing InfoBound techniques enables us to extract meaningful information from unlabeled OoD data, even without explicit semantic labels. In Table 7, we illustrate the details of our newly constructed benchmark dataset.

**Experiment Details** In this paper, we first assess the proposed InfoBound method in the context of a single out-of-distribution (OoD) object detection task. Building upon prior research [51], we leverage the recent DEFORMABLE-DETR (DDETR, [89]) architecture. DDETR introduces multi-scale deformable attention modules in the transformer encoder and decoder layers of DETR [90], and provides better convergence and lower complexity. The multi-scale feature maps in DDETR are extracted from a ResNet-50 pre-trained on ImageNet in a self-supervised fashion, i.e., DINO [91]. Without loss of generality, based on the in-distribution set of BDD-100K and unlabeled semantic-shifted OoD samples (20 samples), we train DDETR using our InfoBound framework as illustrated in Figure 4. During training, we exclusively focus on training specific layers of DDETR, namely the “class embed”, “bbox embed”, and “transformer decoder” layers, while we keep the other layers frozen to facilitate fast convergence. The learning rate is set to 5e-5, with the hyperparameter  $\theta$  fixed at -1, and the coefficient of the InfoBound regularization loss established as 1.0. Subsequently, to assess the efficacy of our InfoBound on addressing two key issues simultaneously, we conduct experiments on our constructed benchmark dataset. In this experiment, we incorporate unlabeled OoD samples consisting of 20 covariate-

TABLE 8: Comparison with competitive out-of-distribution detection methods. All methods are based on the same model backbone DDETR.  $\uparrow$  indicates larger values are better and  $\downarrow$  indicates smaller values are better. Ablations on the vanilla Grounding DINO are also conducted to eliminate the effect of model backbone. All values are percentages. We highlight the **best results** and the second best results. InfoBound results are estimated across 3 runs.

ID Dataset	Method	FPR95 $\downarrow$	AUROC $\uparrow$	mAP (ID) $\uparrow$	ID Dataset	Method	FPR95 $\downarrow$	AUROC $\uparrow$	mAP (ID) $\uparrow$
		OoD: MS-COCO / OpenImages					OoD: MS-COCO / OpenImages		
Backbone: DDETR									
PASCAL-VOC	Mahalanobis [83]	97.39 / 97.88	50.28 / 49.08	60.6	BDD-100K	Mahalanobis [83]	70.86 / 71.43	76.83 / 77.98	31.3
	Gram matrices [84]	94.16 / 95.29	43.97 / 38.81	60.6		Gram matrices [84]	73.81 / 71.56	60.13 / 57.14	31.3
	KNN [47]	91.80 / 91.36	62.15 / 59.64	60.6		KNN [45]	64.75 / 61.13	80.90 / 79.64	31.3
	CSI [85]	84.00 / 79.16	55.07 / 51.37	59.5		CSI [76]	70.27 / 71.30	77.93 / 76.42	29.9
	VOS [50]	97.46 / 97.07	54.40 / 52.77	60.3		VOS [50]	76.44 / 72.58	77.33 / 76.62	31.0
	OW-DETR [86]	93.09 / 93.82	55.70 / 57.80	58.3		OW-DETR [86]	80.78 / 77.37	70.29 / 73.78	28.1
PASCAL-VOC	Dismax [87]	82.05 / 76.37	75.21 / 70.66	60.1	Dismax [87]	77.62 / 81.23	72.14 / 67.18	31.2	
	SIREN-vMF [51]	75.49 / 78.36	76.10 / 71.05	60.8	SIREN-vMF [51]	67.54 / 66.31	80.06 / 79.77	31.3	
	SIREN-KNN [51]	64.77 / 65.99	78.23 / 74.93	60.8	SIREN-KNN [51]	53.97 / 47.28	86.56 / 89.00	31.3	
	SAFE [82]	48.88 / 8.99	78.88 / 96.73	60.6	SAFE [82]	39.18 / 21.10	85.95 / 94.31	31.3	
	<b>InfoBound</b>	<b>44.88 / 43.89</b>	<b>89.76 / 88.00</b>	<b>61.2</b>	<b>InfoBound</b>	<b>23.51 / 25.65</b>	<b>94.97 / 95.60</b>	<b>31.3</b>	

TABLE 9: Benchmark results for both OoD Generalization and OoD Detection. Based on the DDETR, we evaluate the performances of recent state-of-the-art methods following their original papers.

Method	mAP (ID) $\uparrow$	mAP (OoD) $\uparrow$	FPR95 $\downarrow$	AUROC $\uparrow$
		OoD: MS-COCO / OpenImages		
CSI [85]	32.0 / 32.0	32.1 / 32.1	72.1 / 54.5	75.6 / 82.6
VOS [50]	<b>33.3 / 33.3</b>	30.8 / 30.8	70.3 / 56.7	76.9 / 84.2
SIREN-KNN [51]	33.0 / 33.0	31.9 / 31.9	50.0 / 40.4	84.4 / 87.9
SAFE [82]	31.8 / 31.8	33.1 / 33.1	51.1 / 33.7	82.4 / 91.0
<b>InfoBound</b>	32.0 / 32.2	<b>33.9 / 33.8</b>	<b>24.8 / 20.0</b>	<b>95.4 / 96.0</b>

TABLE 10: OoD detection and OoD generalization results of the fine-tuned Grounding DINO with and without InfoBound. All OoD detection results are obtained by inferring KNN [47] ( $k = 500$ ) on box-level embeddings.

OoD Data	Method	mAP (OoD)	mAP (ID)	FPR95	AUROC
MS-COCO	Baseline [88]	36.8	35.6	27.34	94.17
	<b>InfoBound</b>	<b>37.9</b>	<b>36.1</b>	<b>12.29</b>	<b>97.70</b>
OpenImages	Baseline [88]	36.8	35.6	8.81	98.28
	<b>InfoBound</b>	<b>37.8</b>	<b>35.9</b>	<b>2.59</b>	<b>99.27</b>

shifted samples and 20 semantic-shifted samples. We exclusively focus on fine-tuning specific layers of Grounding DINO, namely the “feature map”, “input projection”, and “Transformer decoder” layers. We freeze the other layers to facilitate fast convergence. We set the learning rate to  $1e-4$ , the hyperparameter  $\theta$  to -1, and the coefficient of the InfoBound regularization loss to 4.0. Moreover, to evaluate the effectiveness of our InfoBound on advanced large-scale pre-trained vision-language models, such as Grounding DINO [88], we perform few-shot fine-tuning using 100-shot ID samples on Grounding DINO, both with and without InfoBound. Ablation studies on the sample size of unlabeled OoD samples are also conducted to demonstrate the robustness of our approach. Without specifying otherwise, the OoD detection results for our InfoBound method are obtained using KNN (K-Nearest Neighbors) distance ( $k = 10$ ) during inference.

**Metrics** To evaluate the object detection performance on both the in-distribution data and covariate-shifted OoD data, we employ the common metric mean Average Preci-

sion (mAP). The mAP result on the covariate-shifted OoD data serves as an indicator of the model’s OoD generalization performance. For evaluating the OoD detection performance, we report: (1) the false positive rate (FPR95) of OoD objects when the true positive rate of ID samples is at 95%; (2) the area under the receiver operating characteristic curve (AUROC).

**Experiment Results for the Single OoD Object Detection Task** In Table 8, we present the experiment results on the previous OoD object detection benchmark. Our evaluation includes a comparison of the InfoBound method with competitive OoD detection approaches in the literature, such as Mahalanobis [83], Gram matrices [84], KNN distance [47], CSI [85], as well as previous methods explicitly designed for OoD object detection, including SIREN [51], VOS [50], and SAFE [82]. Our InfoBound method leverages both the MI-Min and CE-Max processes, enabling us to manipulate the distribution of latent embeddings, while regularizing the output logits for object classification through the energy-based loss  $\mathcal{L}_{CE-Max}$ . Notably, from the results in Table 8, InfoBound achieved the highest average AUROC and mAP among the competitive baselines, outperforming methods [51], [50], [82] explicitly designed for OoD object detection. Especially when utilizing BDD-100K as the ID dataset and MS-COCO as the semantic-shifted OoD dataset, InfoBound significantly enhances the FPR95 by up to **15.6%** compared to SAFE [82]. Notably, our InfoBound method achieves improvement in OoD detection performance without compromising its ability to accurately detect objects within the in-distribution dataset. Overall, the results presented in Table 8 highlight that the InfoBound method showcases superior performance compared to competitive baselines, excelling not only in OoD object detection but also in ID object detection.

**Experiment Results for both OoD Generalization and OoD Object Detection** We report the experiment results on both OoD generalization and OoD object detection in Table 9. We mainly compare our InfoBound method with competitive methods explicitly designed for OoD object detection, including VOS [50], SIREN [51], SAFE [82]. As shown in Table 9, although the competitors may achieve slightly higher mAP results on ID data, it comes at the cost of significant performance degradation in OoD generalization or OoD object detection ability. Fortunately, our InfoBound method successfully addresses these limitations

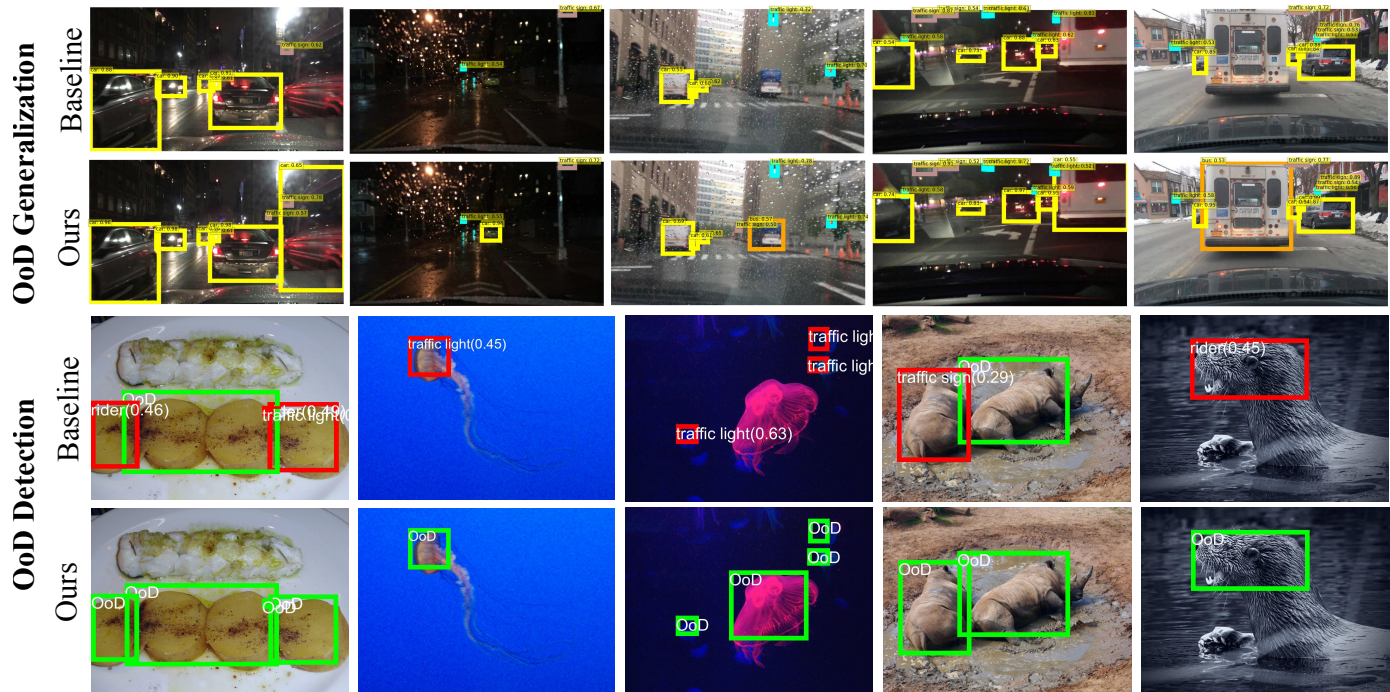


Fig. 7: Qualitative visualization of OoD generalization and OoD detection results based on DDETR. BDD100K is the semantic IN and MS-COCO is the semantic OUT. For the covariate-shifted OoD data, we display the detected objects, using the same color boxes for the same categories. For the semantic-shifted OoD data, OoD objects that are incorrectly classified as semantic IN are highlighted with red boxes, while OoD objects correctly identified as semantic OUT are marked with green boxes. Compared to the baseline, our InfoBound effectively enhances the understanding of semantic IN and semantic OUT. For semantic-in datasets, InfoBound accurately detects objects even in challenging scenarios such as rainy weather or when they are positioned in the corner of the image. Moreover, with semantic-out datasets, InfoBound consistently identifies a greater number of OoD objects compared to the vanilla model.

and showcases robust overall performance in both the OoD generalization and OoD object detection tasks. For example, in the case of using MS-COCO as the semantic-shifted OoD dataset, InfoBound substantially improves the FPR95 result by 26.3% compared with SAFE [82], meanwhile achieving a +0.8% improvement on the OoD generalization performance. The inferior performance of SAFE may be attributed to its vulnerability in cases where OoD semantic-shifted objects exhibit features similar to an ID class. Consequently, SAFE may struggle to effectively discriminate between covariate-shifted and semantic-shifted OoD data, resulting in inferior performance compared to its performance in addressing the single OoD detection task.

**Evaluation on Large-scale Pre-trained Vision-Language Model** Furthermore, to evaluate the effectiveness of our InfoBound on the large-scale pre-trained model, we conduct experiments with the very recent Grounding DINO architecture [88]. Grounding DINO is a strong open-set object detector marrying Transformer-based detector DINO [91] with language pre-training. We show the results on our newly constructed benchmark datasets in Table 10. Compared to results in Table 9, the vanilla fine-tuned Grounding DINO exhibits a superior ability to discriminate between the covariate-shifted and semantic-shifted OoD objects. This improvement also showcases the power of Grounding DINO [88]. Moreover, the notably better results on FPR95 and AU-ROC, when compared to the vanilla fine-tuned Grounding DINO, highlight the superiority of the proposed InfoBound

method on various object detection architectures.

**Visual Explanations** In Figure 7 and Figure 8, we visualize some prediction results on different types of OoD images based on DDETR and Grounding DINO, respectively. We compare models trained with the InfoBound loss against baseline models trained without it. In these figures, the semantic-in data is BDD100K and the semantic OUT OoD data is OpenImages. We can observe that: our InfoBound method demonstrates superior performance compared to the vanilla object detectors in identifying semantic IN objects under various weather conditions. Particularly, when it comes to vehicles located in the corners of the image or in low-light conditions, our method significantly outperforms the baseline. Furthermore, our InfoBound exhibits better identification of semantic-shifted OoD objects (highlighted in green in Figure 7 and Figure 8) compared to the vanilla object detectors, effectively reducing false positives. Overall, by leveraging freely available wild OoD data, our InfoBound method greatly enhances the understanding of semantic IN and semantic OUT, leading to improved OoD generalization and OoD detection performance, even in challenging few-shot object detection tasks.

**Ablation Studies on Sample Size of Unlabeled OoD Data** To demonstrate the robustness of our InfoBound, we also provide ablation results on the sample size of unlabeled OoD data, investigating the impact of varying the amount of unlabeled data on the performance of InfoBound. Keeping the labeled ID training data unchanged, we conduct ex-

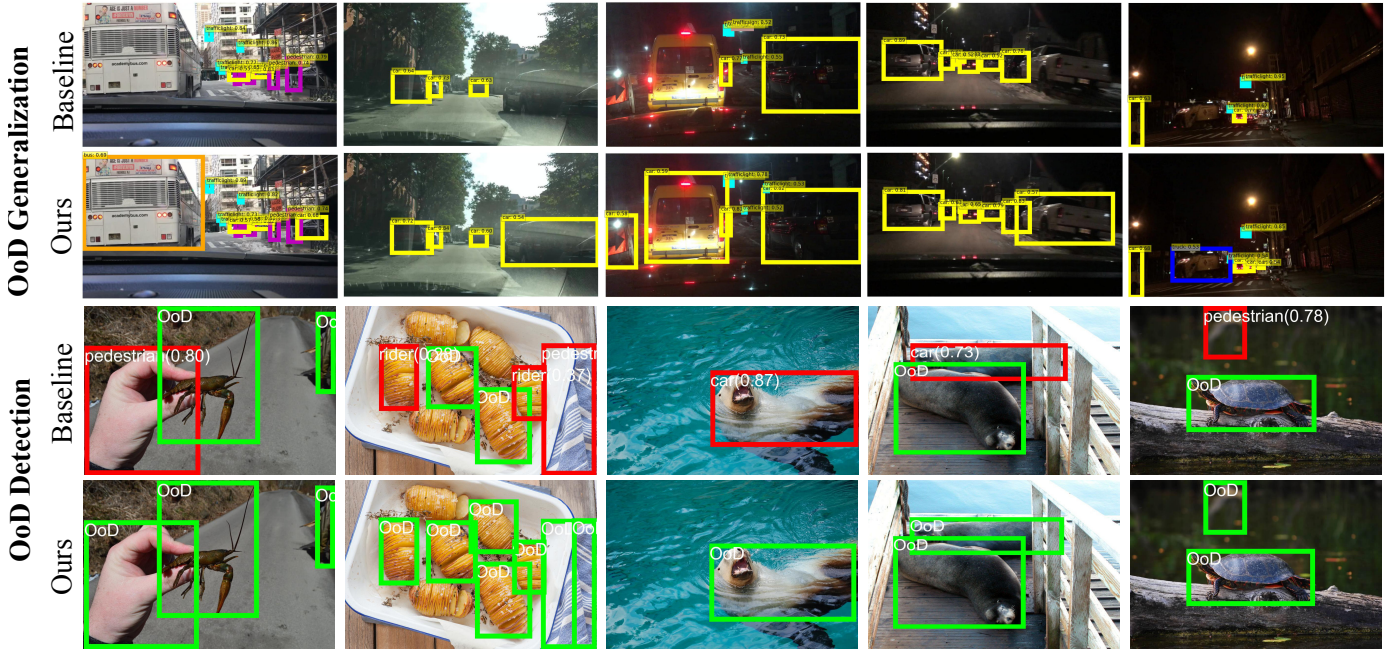


Fig. 8: Visualization of OoD generalization and OoD detection results based on Grounding DINO. BDD100K is the Semantic IN and OpenImages is semantic OUT. For the covariate-shifted OoD data, we display the detected objects, using the same color boxes for the same categories. For the semantic-shifted OoD data, OoD objects that are incorrectly classified as semantic IN are highlighted with red boxes, while OoD objects correctly identified as semantic OUT are marked with green boxes. By exploring the freely available wild data, our InfoBound method successfully captures a better understanding of covariate-shifted OoD data, thus boosting OoD generalization on the advanced Grounding DINO model. For instance, our method demonstrates superior performance compared to the vanilla model when identifying vehicles positioned in the corner of the image or in low-light conditions. Furthermore, InfoBound excels in identifying semantic-shifted OoD objects compared to the vanilla fine-tuned Grounding DINO model.

TABLE 11: Ablation Study Results on Sample Size of Unlabeled Data. All OoD detection results are obtained by inferring KNN [47] ( $k = 5$ ) on box-level embeddings. Even with a 2-shot unlabeled OoD data, our InfoBound achieved significant improvements on both tasks.

OoD Data	Method	mAP(OoD)	mAP(ID)	FPR	AUROC
MS-COCO	Baseline [88]	36.8	35.6	17.63	95.82
	<b>InfoBound</b> ( $N = 20$ )	<b>37.9</b>	<b>36.1</b>	4.44	99.04
	<b>InfoBound</b> ( $N = 5$ )	37.2	35.6	4.29	99.04
	<b>InfoBound</b> ( $N = 2$ )	37.2	35.6	<b>4.11</b>	<b>99.08</b>
OpenImages	Baseline [88]	36.8	35.6	2.37	99.20
	<b>InfoBound</b> ( $N = 20$ )	37.8	35.9	0.69	99.67
	<b>InfoBound</b> ( $N = 5$ )	<b>38.1</b>	<b>36.2</b>	0.99	99.57
	<b>InfoBound</b> ( $N = 2$ )	37.7	35.7	<b>0.25</b>	<b>99.85</b>

periments using three different numbers of unlabeled OoD data, with the few-shot numbers, denoted as  $N$ , ranging in [2-shot, 5-shot, 20-shot]. Note that in the case of “ $N$ -shot” unlabeled OoD samples, it indicates that there are a total of  $N$  unlabeled examples that exhibit covariate shifts and a total of  $N$  unlabeled examples that demonstrate semantic shifts during the training process. As shown in Table 11, under different numbers of unlabeled OoD data, our InfoBound method achieves robust improvements over fine-tuning the GroundingDINO model without InfoBound loss. Notably, even with a 2-shot unlabeled OoD data, our InfoBound can achieve significant improvements on both

tasks. This demonstrates that InfoBound achieves robust enhancement on both tasks even with partial categories from unlabeled OoD data, highlighting its robustness across varying sample sizes of unlabeled OoD data.

Furthermore, we present the OoD detection results of both the baseline model and our InfoBound method using different KNN distances on the box-level representations. Figure 9 illustrates that our InfoBound consistently achieves significantly better performance compared to the baseline as the number of neighbors, represented as  $k$ , increases. This improvement is observed across various sample sizes of unlabeled OoD data. These results highlight the effectiveness of our proposed MI-Min process in effectively differentiating between representations of semantic IN and semantic OUT. Additionally, the comparison between the baseline model and the proposed InfoBound emphasizes the specific advantages provided by our representation reshaping loss  $\mathcal{L}_{MI-Min}$ .

In conclusion, our extensive experiments serve as strong evidence that incorporating the proposed InfoBound framework into the training process produces tangible benefits. By leveraging freely available few-shot unlabeled data and the pre-trained model, we achieved notable enhancements in both OoD generalization and OoD detection. This finding also demonstrates the potential of InfoBound in refining and elevating the capabilities of large-scale pre-trained models, like the awesome GroundingDINO model. We believe this information will be valuable for researchers and practition-

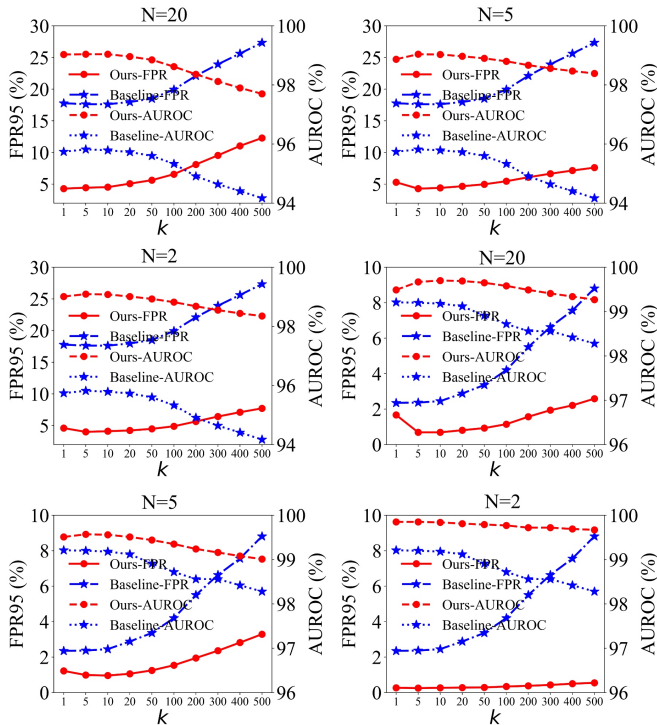


Fig. 9: OoD detection results of the baseline model and our InfoBound by referring to KNN distances on the box-level embeddings. The first three images correspond to detecting MS-COCO, while the latter three images correspond to detecting OpenImages. With the increase of  $k$ , our InfoBound outperforms the baseline by a large margin under various sample sizes of the unlabeled OoD data.

ers interested in leveraging unlabeled data and the proposed InfoBound techniques to improve the performance of large-scale pre-trained models.

## 5 CONCLUSION

We have proposed a novel bound optimization-based method to address both covariate shifts and semantic shifts, which formalizes the OoD generalization and OoD detection from a novel information theory perspective. Under mild assumptions, our InfoBound method has demonstrated significantly lower prediction errors on covariate-shifted OoD data compared to ERM, meanwhile excels in distinguishing semantic IN and semantic OUT. Moreover, we provide an in-depth analysis demonstrating the superiority of InfoBound in mitigating the trade-off between OoD generalization and OoD detection. Extensive empirical experiments and ablation studies further validate the effectiveness of InfoBound, addressing a previously underexplored challenge in balancing OoD generalization and OoD detection performance.

## REFERENCES

[1] N. Meinshausen and P. Bühlmann, “Maximin effects in inhomogeneous large-scale data,” *The Annals of Statistics*, vol. 43, no. 4, aug 2015. [Online]. Available: <https://doi.org/10.1214/2F15-aos1325>

[2] P. W. Koh, S. Sagawa, H. Marklund, S. M. Xie, M. Zhang, A. Balsubramani, W. Hu, M. Yasunaga, R. L. Phillips, S. Beery *et al.*, “Wilds: A benchmark of in-the-wild distribution shifts,” *arXiv:2012.07421*, 2020.

[3] H. Wang, C. Zhao, Y. Guo, K. Jiang, and F. Chen, “Towards effective semantic ood detection in unseen domains: A domain generalization perspective,” *arXiv preprint arXiv:2309.10209*, 2023.

[4] H. Bai, G. Canal, X. Du, J. Kwon, R. D. Nowak, and Y. Li, “Feed two birds with one scone: Exploiting wild data for both out-of-distribution generalization and detection,” in *International Conference on Machine Learning*. PMLR, 2023, pp. 1454–1471.

[5] J. Ren, P. J. Liu, E. Fertig, J. Snoek, R. Poplin, M. Depristo, J. Dillon, and B. Lakshminarayanan, “Likelihood ratios for out-of-distribution detection,” *Advances in neural information processing systems*, vol. 32, 2019.

[6] J. Ren, S. Fort, J. Liu, A. G. Roy, S. Padhy, and B. Lakshminarayanan, “A simple fix to mahalanobis distance for improving near-ood detection,” *arXiv preprint arXiv:2106.09022*, 2021.

[7] J. Winkens, R. Bunel, A. G. Roy, R. Stanforth, V. Natarajan, J. R. Ledsam, P. MacWilliams, P. Kohli, A. Karthikesalingam, S. Kohl *et al.*, “Contrastive training for improved out-of-distribution detection,” *arXiv preprint arXiv:2007.05566*, 2020.

[8] W. Liu, X. Wang, J. Owens, and Y. Li, “Energy-based out-of-distribution detection,” *Advances in neural information processing systems*, vol. 33, pp. 21 464–21 475, 2020.

[9] J. Katz-Samuels, J. B. Nakhleh, R. Nowak, and Y. Li, “Training ood detectors in their natural habitats,” in *International Conference on Machine Learning*. PMLR, 2022, pp. 10 848–10 865.

[10] K. Muandet, D. Balduzzi, and B. Schölkopf, “Domain generalization via invariant feature representation,” in *International Conference on Machine Learning*. PMLR, 2013, pp. 10–18.

[11] K. Akuzawa, Y. Iwasawa, and Y. Matsuo, “Adversarial invariant feature learning with accuracy constraint for domain generalization,” in *Joint European Conference on Machine Learning and Knowledge Discovery in Databases*. Springer, 2019, pp. 315–331.

[12] C. Lu, Y. Wu, J. M. Hernández-Lobato, and B. Schölkopf, “Invariant causal representation learning for out-of-distribution generalization,” in *International Conference on Learning Representations*, 2021.

[13] P. Stojanov, Z. Li, M. Gong, R. Cai, J. Carbonell, and K. Zhang, “Domain adaptation with invariant representation learning: What transformations to learn?” *Advances in Neural Information Processing Systems*, vol. 34, pp. 24 791–24 803, 2021.

[14] M. Arjovsky, L. Bottou, I. Gulrajani, and D. Lopez-Paz, “Invariant risk minimization,” *arXiv preprint arXiv:1907.02893*, 2019.

[15] C. Song, K. He, L. Wang, and J. E. Hopcroft, “Improving the generalization of adversarial training with domain adaptation,” *arXiv preprint arXiv:1810.00740*, 2018.

[16] H. Li, S. J. Pan, S. Wang, and A. C. Kot, “Domain generalization with adversarial feature learning,” in *Proceedings of the IEEE conference on computer vision and pattern recognition*, 2018, pp. 5400–5409.

[17] Z. Huang, H. Wang, E. P. Xing, and D. Huang, “Self-challenging improves cross-domain generalization,” *arXiv:2007.02454*, 2020.

[18] Q. Dou, D. Coelho de Castro, K. Kamnitsas, and B. Glocker, “Domain generalization via model-agnostic learning of semantic features,” *Advances in Neural Information Processing Systems*, vol. 32, 2019.

[19] D. Peng and S. J. Pan, “Learning gradient-based mixup towards flatter minima for domain generalization,” *arXiv preprint arXiv:2209.14742*, 2022.

[20] H. Bai, R. Sun, L. Hong, F. Zhou, N. Ye, H.-J. Ye, S.-H. G. Chan, and Z. Li, “Decaug: Out-of-distribution generalization via decomposed feature representation and semantic augmentation,” in *Proceedings of the AAAI Conference on Artificial Intelligence*, vol. 35, no. 8, 2021, pp. 6705–6713.

[21] Y. Du, J. Xu, H. Xiong, Q. Qiu, X. Zhen, C. G. Snoek, and L. Shao, “Learning to learn with variational information bottleneck for domain generalization,” in *Computer Vision—ECCV 2020: 16th European Conference, Glasgow, UK, August 23–28, 2020, Proceedings, Part X 16*. Springer, 2020, pp. 200–216.

[22] D. Li, Y. Yang, Y.-Z. Song, and T. Hospedales, “Learning to generalize: Meta-learning for domain generalization,” in *Proceedings of the AAAI conference on artificial intelligence*, vol. 32, no. 1, 2018.

[23] C. Finn, P. Abbeel, and S. Levine, “Model-agnostic meta-learning for fast adaptation of deep networks,” in *International conference on machine learning*. PMLR, 2017, pp. 1126–1135.

- [24] M. Rojas-Carulla, B. Schölkopf, R. Turner, and J. Peters, "Invariant models for causal transfer learning," *The Journal of Machine Learning Research*, vol. 19, no. 1, pp. 1309–1342, 2018.
- [25] G. Blanchard, A. A. Deshmukh, Ü. Dogan, G. Lee, and C. Scott, "Domain generalization by marginal transfer learning," *The Journal of Machine Learning Research*, vol. 22, no. 1, pp. 46–100, 2021.
- [26] J. Wang, C. Lan, C. Liu, Y. Ouyang, and T. Qin, "Generalizing to unseen domains: A survey on domain generalization," *CoRR*, vol. abs/2103.03097, 2021. [Online]. Available: <https://arxiv.org/abs/2103.03097>
- [27] Z. Shen, P. Cui, T. Zhang, and K. Kuang, "Stable learning via sample reweighting," 2019.
- [28] D. Arpit, H. Wang, Y. Zhou, and C. Xiong, "Ensemble of averages: Improving model selection and boosting performance in domain generalization," *Advances in Neural Information Processing Systems*, vol. 35, pp. 8265–8277, 2022.
- [29] Y. Lin, H. Dong, H. Wang, and T. Zhang, "Bayesian invariant risk minimization," in *Proceedings of the IEEE/CVF Conference on Computer Vision and Pattern Recognition*, 2022, pp. 16 021–16 030.
- [30] I. Gulrajani and D. Lopez-Paz, "In search of lost domain generalization," in *ICLR*, 2021.
- [31] N. Ye, K. Li, L. Hong, H. Bai, Y. Chen, F. Zhou, and Z. Li, "Ood-bench: Benchmarking and understanding out-of-distribution generalization datasets and algorithms," *CoRR*, vol. abs/2106.03721, 2021. [Online]. Available: <https://arxiv.org/abs/2106.03721>
- [32] Y. Ding, L. Wang, B. Liang, S. Liang, Y. Wang, and F. Chen, "Domain generalization by learning and removing domain-specific features," 2022.
- [33] M. Ghifary, W. B. Kleijn, M. Zhang, and D. Balduzzi, "Domain generalization for object recognition with multi-task autoencoders," 2015.
- [34] P. Chattopadhyay, Y. Balaji, and J. Hoffman, "Learning to balance specificity and invariance for in and out of domain generalization," in *Computer Vision—ECCV 2020: 16th European Conference, Glasgow, UK, August 23–28, 2020, Proceedings, Part IX 16*. Springer, 2020, pp. 301–318.
- [35] J. Cha, K. Lee, S. Park, and S. Chun, "Domain generalization by mutual-information regularization with pre-trained models," in *European Conference on Computer Vision*. Springer, 2022, pp. 440–457.
- [36] T. Steinke and L. Zakyntinou, "Reasoning about generalization via conditional mutual information," in *Conference on Learning Theory*. PMLR, 2020, pp. 3437–3452.
- [37] C. Zhao and W. Shen, "Adversarial mutual information-guided single domain generalization network for intelligent fault diagnosis," *IEEE Transactions on Industrial Informatics*, vol. 19, no. 3, pp. 2909–2918, 2022.
- [38] X. Yang, H. Zhang, G. Qi, and J. Cai, "Causal attention for vision-language tasks," in *2021 IEEE/CVF Conference on Computer Vision and Pattern Recognition (CVPR)*, 2021, pp. 9842–9852.
- [39] T. Wang, C. Zhou, Q. Sun, and H. Zhang, "Causal attention for unbiased visual recognition," in *2021 IEEE/CVF International Conference on Computer Vision (ICCV)*, 2021, pp. 3071–3080.
- [40] K. Nadjahi, K. Greenewald, R. B. Gabrielsson, and J. Solomon, "Slicing mutual information generalization bounds for neural networks," *arXiv preprint arXiv:2406.04047*, 2024.
- [41] T. Nguyen, B. Lyu, P. Ishwar, M. Scheutz, and S. Aeron, "Conditional entropy minimization principle for learning domain invariant representation features," in *2022 26th International Conference on Pattern Recognition (ICPR)*. IEEE, 2022, pp. 3000–3006.
- [42] Y. Zhu, Y. Chen, C. Xie, X. Li, R. Zhang, H. Xue, X. Tian, Y. Chen *et al.*, "Boosting out-of-distribution detection with typical features," *Advances in Neural Information Processing Systems*, vol. 35, pp. 20 758–20 769, 2022.
- [43] Y. Sun, C. Guo, and Y. Li, "React: Out-of-distribution detection with rectified activations," *Advances in Neural Information Processing Systems*, vol. 34, pp. 144–157, 2021.
- [44] D. Hendrycks and K. Gimpel, "A baseline for detecting misclassified and out-of-distribution examples in neural networks," *arXiv preprint arXiv:1610.02136*, 2016.
- [45] S. Liang, Y. Li, and R. Srikant, "Enhancing the reliability of out-of-distribution image detection in neural networks," *arXiv preprint arXiv:1706.02690*, 2017.
- [46] H. Wang, Z. Li, L. Feng, and W. Zhang, "Vim: Out-of-distribution with virtual-logit matching," in *Proceedings of the IEEE/CVF conference on computer vision and pattern recognition*, 2022, pp. 4921–4930.
- [47] Y. Sun, Y. Ming, X. Zhu, and Y. Li, "Out-of-distribution detection with deep nearest neighbors," in *International Conference on Machine Learning*. PMLR, 2022, pp. 20 827–20 840.
- [48] V. Narayanaswamy, Y. Mubarka, R. Anirudh, D. Rajan, and J. J. Thiagarajan, "Exploring inlier and outlier specification for improved medical ood detection," in *Proceedings of the IEEE/CVF International Conference on Computer Vision (ICCV) Workshops*, October 2023, pp. 4589–4598.
- [49] A. Malinin and M. Gales, "Predictive uncertainty estimation via prior networks," *Advances in neural information processing systems*, vol. 31, 2018.
- [50] X. Du, Z. Wang, M. Cai, and Y. Li, "Vos: Learning what you don't know by virtual outlier synthesis," *arXiv preprint arXiv:2202.01197*, 2022.
- [51] X. Du, G. Gozum, Y. Ming, and Y. Li, "Siren: Shaping representations for detecting out-of-distribution objects," *Advances in Neural Information Processing Systems*, vol. 35, pp. 20 434–20 449, 2022.
- [52] Y. Ming, Y. Fan, and Y. Li, "Poem: Out-of-distribution detection with posterior sampling," in *International Conference on Machine Learning*. PMLR, 2022, pp. 15 650–15 665.
- [53] J. Huang, S. Gong, and X. Zhu, "Deep semantic clustering by partition confidence maximisation," in *Proceedings of the IEEE/CVF conference on computer vision and pattern recognition*, 2020, pp. 8849–8858.
- [54] X. Ji, J. F. Henriques, and A. Vedaldi, "Invariant information clustering for unsupervised image classification and segmentation," in *Proceedings of the IEEE/CVF international conference on computer vision*, 2019, pp. 9865–9874.
- [55] X. Peng, H. Zhu, J. Feng, C. Shen, H. Zhang, and J. T. Zhou, "Deep clustering with sample-assignment invariance prior," *IEEE transactions on neural networks and learning systems*, vol. 31, no. 11, pp. 4857–4868, 2019.
- [56] T. Chen, S. Kornblith, M. Norouzi, and G. Hinton, "A simple framework for contrastive learning of visual representations," in *International conference on machine learning*. PMLR, 2020, pp. 1597–1607.
- [57] J. Li, P. Zhou, C. Xiong, and S. C. Hoi, "Prototypical contrastive learning of unsupervised representations," in *ICLR*, 2021.
- [58] M. Caron, I. Misra, J. Mairal, P. Goyal, P. Bojanowski, and A. Joulin, "Unsupervised learning of visual features by contrasting cluster assignments," *Advances in neural information processing systems*, vol. 33, pp. 9912–9924, 2020.
- [59] T. Wang and P. Isola, "Understanding contrastive representation learning through alignment and uniformity on the hypersphere," in *International Conference on Machine Learning*. PMLR, 2020, pp. 9929–9939.
- [60] A. Krizhevsky, G. Hinton *et al.*, "Learning multiple layers of features from tiny images," 2009.
- [61] D. Hendrycks and T. Dietterich, "Benchmarking neural network robustness to common corruptions and perturbations," in *ICLR*, 2019.
- [62] N. Yuval, "Reading digits in natural images with unsupervised feature learning," in *Proceedings of the NIPS Workshop on Deep Learning and Unsupervised Feature Learning*, 2011.
- [63] M. Cimpoi, S. Maji, I. Kokkinos, S. Mohamed, and A. Vedaldi, "Describing textures in the wild," in *Proceedings of the IEEE conference on computer vision and pattern recognition*, 2014, pp. 3606–3613.
- [64] F. Yu, A. Seff, Y. Zhang, S. Song, T. Funkhouser, and J. Xiao, "Lsun: Construction of a large-scale image dataset using deep learning with humans in the loop," *arXiv preprint arXiv:1506.03365*, 2015.
- [65] G. Van Horn, O. Mac Aodha, Y. Song, Y. Cui, C. Sun, A. Shepard, H. Adam, P. Perona, and S. Belongie, "The naturalist species classification and detection dataset," in *Proceedings of the IEEE conference on computer vision and pattern recognition*, 2018, pp. 8769–8778.
- [66] K. He, X. Zhang, S. Ren, and J. Sun, "Deep residual learning for image recognition," in *Proceedings of the IEEE conference on computer vision and pattern recognition*, 2016, pp. 770–778.
- [67] A. Radford, J. W. Kim, C. Hallacy, A. Ramesh, G. Goh, S. Agarwal, G. Sastry, A. Askell, P. Mishkin, J. Clark, G. Krueger, and I. Sutskever, "Learning transferable visual models from natural language supervision," *CoRR*, vol. abs/2103.00020, 2021. [Online]. Available: <https://arxiv.org/abs/2103.00020>
- [68] K. Zhou, J. Yang, C. C. Loy, and Z. Liu, "Learning to prompt for vision-language models," *arXiv preprint arXiv:2109.01134*, 2021.

- [69] P. Gao, S. Geng, R. Zhang, T. Ma, R. Fang, Y. Zhang, H. Li, and Y. Qiao, "Clip-adapter: Better vision-language models with feature adapters," *arXiv preprint arXiv:2110.04544*, 2021.
- [70] L. Zhu, W. Yin, Y. Yang, F. Wu, Z. Zeng, Q. Gu, X. Wang, C. Zhou, and N. Ye, "Vision-language alignment learning under affinity and divergence principles for few-shot out-of-distribution generalization," *International Journal of Computer Vision*, pp. 1–33, 2024.
- [71] X. Zhang, Y. Iwasawa, Y. Matsuo, and S. S. Gu, "Amortized prompt: Guide clip to domain transfer learning," *arXiv preprint arXiv:2111.12853*, 2021.
- [72] J. Deng, W. Dong, R. Socher, L.-J. Li, K. Li, and L. Fei-Fei, "Imagenet: A large-scale hierarchical image database," in *2009 IEEE Conference on Computer Vision and Pattern Recognition*, 2009, pp. 248–255.
- [73] D. Hendrycks, K. Zhao, S. Basart, J. Steinhardt, and D. Song, "Natural adversarial examples," in *Proceedings of the IEEE/CVF Conference on Computer Vision and Pattern Recognition*, 2021, pp. 15 262–15 271.
- [74] D. Hendrycks, S. Basart, N. Mu, S. Kadavath, F. Wang, E. Dorundo, R. Desai, T. Zhu, S. Parajuli, M. Guo *et al.*, "The many faces of robustness: A critical analysis of out-of-distribution generalization," in *Proceedings of the IEEE/CVF International Conference on Computer Vision*, 2021, pp. 8340–8349.
- [75] H. Wang, S. Ge, Z. Lipton, and E. P. Xing, "Learning robust global representations by penalizing local predictive power," *Advances in Neural Information Processing Systems*, vol. 32, 2019.
- [76] B. Recht, R. Roelofs, L. Schmidt, and V. Shankar, "Do imagenet classifiers generalize to imagenet?" in *International conference on machine learning*. PMLR, 2019, pp. 5389–5400.
- [77] M. Everingham, L. Van Gool, C. K. Williams, J. Winn, and A. Zisserman, "The pascal visual object classes (voc) challenge," *International journal of computer vision*, vol. 88, pp. 303–338, 2010.
- [78] F. Yu, H. Chen, X. Wang, W. Xian, Y. Chen, F. Liu, V. Madhavan, and T. Darrell, "Bdd100k: A diverse driving dataset for heterogeneous multitask learning," in *Proceedings of the IEEE/CVF conference on computer vision and pattern recognition*, 2020, pp. 2636–2645.
- [79] T.-Y. Lin, M. Maire, S. Belongie, J. Hays, P. Perona, D. Ramanan, P. Dollár, and C. L. Zitnick, "Microsoft coco: Common objects in context," in *Computer Vision—ECCV 2014: 13th European Conference, Zurich, Switzerland, September 6–12, 2014, Proceedings, Part V 13*. Springer, 2014, pp. 740–755.
- [80] A. Kuznetsova, H. Rom, N. Alldrin, J. Uijlings, I. Krasin, J. Pont-Tuset, S. Kamali, S. Popov, M. Mallocci, A. Kolesnikov *et al.*, "The open images dataset v4: Unified image classification, object detection, and visual relationship detection at scale," *International Journal of Computer Vision*, vol. 128, no. 7, pp. 1956–1981, 2020.
- [81] F. Wu, N. Ye, H. Lanqing, C. Peng, B. Pan, H. Lyu, and H. Shi, "Detectbench: An object detection benchmark for ood generalization algorithms," 2022.
- [82] S. Wilson, T. Fischer, F. Dayoub, D. Miller, and N. Sünderhauf, "Safe: Sensitivity-aware features for out-of-distribution object detection," in *Proceedings of the IEEE/CVF International Conference on Computer Vision*, 2023, pp. 23 565–23 576.
- [83] K. Lee, K. Lee, H. Lee, and J. Shin, "A simple unified framework for detecting out-of-distribution samples and adversarial attacks," *Advances in neural information processing systems*, vol. 31, 2018.
- [84] C. S. Sastry and S. Oore, "Detecting out-of-distribution examples with gram matrices," in *International Conference on Machine Learning*. PMLR, 2020, pp. 8491–8501.
- [85] J. Tack, S. Mo, J. Jeong, and J. Shin, "Csi: Novelty detection via contrastive learning on distributionally shifted instances," *Advances in neural information processing systems*, vol. 33, pp. 11 839–11 852, 2020.
- [86] A. Gupta, S. Narayan, K. Joseph, S. Khan, F. S. Khan, and M. Shah, "Ow-detr: Open-world detection transformer," in *Proceedings of the IEEE/CVF Conference on Computer Vision and Pattern Recognition*, 2022, pp. 9235–9244.
- [87] D. Macêdo, C. Zanchettin, and T. Ludermit, "Distinction maximization loss: Efficiently improving out-of-distribution detection and uncertainty estimation by replacing the loss and calibrating," *arXiv preprint arXiv:2205.05874*, p. 40, 2022.
- [88] S. Liu, Z. Zeng, T. Ren, F. Li, H. Zhang, J. Yang, C. Li, J. Yang, H. Su, J. Zhu *et al.*, "Grounding dino: Marrying dino with grounded pre-training for open-set object detection," *arXiv preprint arXiv:2303.05499*, 2023.
- [89] X. Zhu, W. Su, L. Lu, B. Li, X. Wang, and J. Dai, "Deformable detr: Deformable transformers for end-to-end object detection," *arXiv preprint arXiv:2010.04159*, 2020.
- [90] N. Carion, F. Massa, G. Synnaeve, N. Usunier, A. Kirillov, and S. Zagoruyko, "End-to-end object detection with transformers," in *European conference on computer vision*. Springer, 2020, pp. 213–229.
- [91] H. Zhang, F. Li, S. Liu, L. Zhang, H. Su, J. Zhu, L. M. Ni, and H.-Y. Shum, "Dino: Detr with improved denoising anchor boxes for end-to-end object detection," *arXiv preprint arXiv:2203.03605*, 2022.
- [92] D. Hendrycks and T. Dietterich, "Benchmarking neural network robustness to common corruptions and perturbations," *arXiv preprint arXiv:1903.12261*, 2019.
- [93] A. Kumar, A. Raghunathan, R. Jones, T. Ma, and P. Liang, "Fine-tuning can distort pretrained features and underperform out-of-distribution," *arXiv preprint arXiv:2202.10054*, 2022.



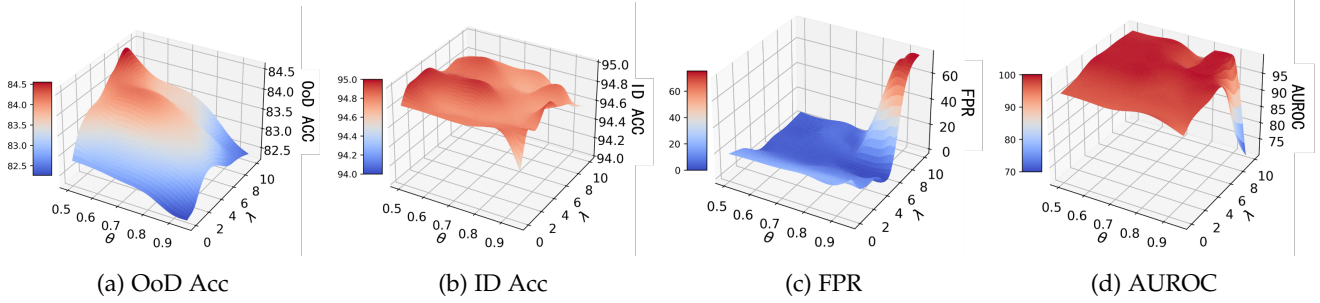


Fig. 10: The sensitivity of InfoBound to hyperparameters  $\theta$  and  $\lambda$ . (The additional hyperparameters introduced by InfoBound are the threshold  $\theta$  in the pseudo-label generator and the coefficient  $\lambda$  of loss function  $\mathcal{L}_{MI-Min} + \mathcal{L}_{CE-Max}$ .) It is observed that the higher OoD accuracies concentrated on the areas with a larger coefficient of the proposed  $\mathcal{L}_{MI-Min} + \mathcal{L}_{CE-Max}$ , which demonstrates the efficacy of our MI-Min and CE-Max processes.

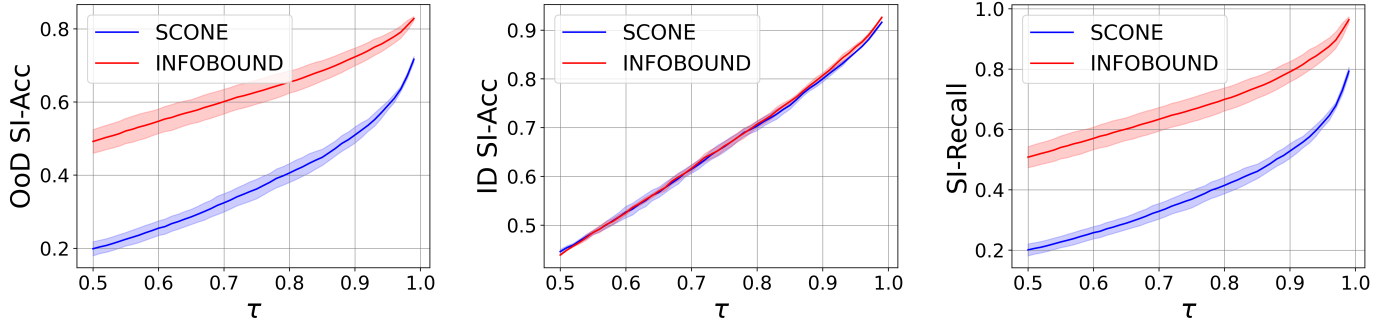


Fig. 11: Ablations on the threshold  $\tau$  in comprehensive evaluation. Under different settings of the threshold  $\tau$ , our proposed InfoBound consistently incorporates more semantic-in samples into the classification process, achieving significant improvements in classification accuracy for both ID data and covariate-shifted OoD data.

## APPENDIX

### .1 Ablations on Other Types of Covariate Shifts

In this section, we offer ablation studies focusing on different types of covariate shifts. In Table 12, we evaluate our method under 19 different common corruptions such as Gaussian noise, defocus blur, glass blur, impulse noise, shot noise, snow, zoom blur, brightness, etc. The corruptions were generated following the default design and parameter settings from the original paper [92]. According to Table 12, in comparison to the state-of-the-art SCONE results, our InfoBound demonstrates a significant advantage in terms of FPR and AUROC for most corruption types. Additionally, our InfoBound performs on par with SCONE in terms of in-distribution accuracy (ID Acc) and out-of-distribution Accuracy (OoD Acc). Notably, for the “frosted glass Blur” corruption type, where SCONE achieves an OoD Acc of 69.32%, our InfoBound consistently maintains a level above 90%. This highlights the superior generalization capability of our method. According to the results in SCONE’s original paper, while SCONE is more robust than the WOODS baseline under various covariate shifts, it sacrifices OoD detection for improved OoD generalization. However, our method significantly enhances OoD detection while still achieving strong OoD generalization performances in diverse covariate shift scenarios, consistently addressing the trade-off of SCONE between OoD generalization and OoD detection.

### .2 Sensitivity to Hyperparameters

For the main experiments in the context of image classification, the additional hyperparameters introduced by InfoBound are the threshold  $\theta$  in the pseudo-label generator and the coefficient  $\lambda$  of loss function  $\mathcal{L}_{MI-Min} + \mathcal{L}_{CE-Max}$ , which is chosen in  $[1, 2, \dots, 10]$  maximizing the accuracy on validation sets. To investigate the sensitivity of InfoBound to these hyperparameters, we varied the values of  $\theta$  and  $\lambda$ . For  $\theta$ , we explored values from 0.5 to 1.0 with a granularity of 0.1, and for  $\lambda$ , we considered values from 1 to 10 with a granularity of 1. By interpolation fitting, we have generated the 3D surface plots in Figure 10, which illustrate the relationship between the model’s performance and the variations in these hyperparameters. We observe that the model demonstrates moderate robustness when  $\theta$  falls within the range of 0.5 to 0.8, which suggests the appropriate range of  $\theta$  to ensure the high quality of pseudo labels.

### .3 Ablations on the Threshold in Comprehensive Evaluation

In this section, we conduct ablation studies focusing on investigating the impact of the threshold  $\tau$  (as defined in Equation 11-13) on the comprehensive evaluation results in Table 2. The experiments are conducted based on the same configuration, where CIFAR-10 serves as the in-distribution dataset, CIFAR-10-C is used as the covariate out-of-distribution dataset, and SVHN is employed as the

TABLE 12: For ablation studies on various types of covariate shifts, we employ CIFAR-10 as the in-distribution dataset, various corruption types from CIFAR-10-C for out-of-distribution covariate shifts (with  $\pi_c = 0.5$ ), and SVHN for out-of-distribution semantic shifts (with  $\pi_s = 0.1$ ). SCONE sacrifices OoD detection for improved OoD generalization. However, our InfoBound method significantly enhances OoD detection while still achieving strong OoD generalization performances in diverse covariate shift scenarios, consistently addressing the trade-off of SCONE between OoD generalization and OoD detection.

Covariate shift type	Method	OOD Acc.↑	ID Acc.↑	FPR↓	AUROC↑
Gaussian noise	INFOBOUND	84.59	<b>94.85</b>	<b>2.64</b>	<b>99.50</b>
Gaussian noise	SCONE	<b>84.69</b>	94.65	10.86	97.84
Defocus blur	INFOBOUND	<b>94.86</b>	<b>94.97</b>	<b>1.05</b>	<b>99.81</b>
Defocus blur	SCONE	<b>94.86</b>	94.92	11.19	97.81
Frosted glass blur	INFOBOUND	<b>91.17</b>	<b>94.63</b>	<b>9.22</b>	<b>98.05</b>
Frosted glass blur	SCONE	69.32	94.49	12.80	97.51
Impulse noise	INFOBOUND	87.34	<b>94.83</b>	<b>6.85</b>	<b>98.58</b>
Impulse noise	SCONE	<b>87.97</b>	94.82	9.70	97.98
Shot noise	INFOBOUND	88.51	<b>94.96</b>	<b>4.65</b>	<b>99.10</b>
Shot noise	SCONE	<b>88.62</b>	94.68	10.74	97.85
Snow	INFOBOUND	90.36	94.82	<b>3.76</b>	<b>99.24</b>
Snow	SCONE	<b>90.85</b>	<b>94.83</b>	13.22	97.32
Zoom blur	INFOBOUND	88.28	<b>94.92</b>	<b>3.45</b>	<b>99.33</b>
Zoom blur	SCONE	<b>90.87</b>	94.89	7.72	98.54
Brightness	INFOBOUND	<b>94.94</b>	94.90	<b>0.70</b>	<b>99.88</b>
Brightness	SCONE	94.93	<b>94.97</b>	1.41	99.74
Elastic transform	INFOBOUND	90.44	<b>94.90</b>	<b>6.44</b>	<b>98.74</b>
Elastic transform	SCONE	<b>91.01</b>	94.88	8.77	98.32
Contrast	INFOBOUND	94.37	94.94	<b>1.06</b>	<b>99.80</b>
Contrast	SCONE	<b>94.40</b>	<b>94.98</b>	1.30	99.77
Fog	INFOBOUND	<b>94.81</b>	94.88	<b>0.85</b>	<b>99.84</b>
Fog	SCONE	94.71	<b>95.00</b>	1.35	99.76
Frost	INFOBOUND	91.30	94.76	<b>5.10</b>	<b>98.97</b>
Frost	SCONE	<b>91.94</b>	<b>94.85</b>	10.08	98.03
Gaussian blur	INFOBOUND	<b>94.79</b>	<b>94.91</b>	<b>2.92</b>	<b>99.44</b>
Gaussian blur	SCONE	94.76	94.86	3.14	99.39
Jpeg	INFOBOUND	87.73	94.87	<b>3.63</b>	<b>99.27</b>
Jpeg	SCONE	<b>87.87</b>	<b>94.90</b>	8.14	98.49
Motion blur	INFOBOUND	91.36	<b>94.95</b>	<b>8.90</b>	98.12
Motion blur	SCONE	<b>91.95</b>	94.90	9.15	<b>98.18</b>
Pixelate	INFOBOUND	<b>93.10</b>	94.84	<b>1.66</b>	<b>99.67</b>
Pixelate	SCONE	92.08	<b>94.96</b>	1.97	99.64
Saturate	INFOBOUND	93.10	94.90	<b>6.13</b>	<b>98.63</b>
Saturate	SCONE	<b>93.38</b>	<b>94.92</b>	10.27	97.88
Spatter	INFOBOUND	92.73	94.66	2.79	99.46
Spatter	SCONE	<b>92.78</b>	<b>94.98</b>	<b>1.94</b>	<b>99.64</b>
Speckle noise	INFOBOUND	88.33	94.79	<b>2.29</b>	<b>99.56</b>
Speckle noise	SCONE	<b>88.51</b>	<b>94.83</b>	11.05	97.82

semantic out-of-distribution dataset, using various metrics proposed in Equations 11-13. The threshold  $\tau$  in Equations 11-13 is varied incrementally, ranging from 0.5 to 0.99, ensuring  $100\% \times \tau$  of the samples from the in-distribution validation set are correctly classified as semantic-in data. By changing  $\tau$  in this manner, we can explore how threshold values affect the model’s overall performance in OoD generalization and OoD detection. This comprehensive evaluation provides insights into the behaviour and effectiveness of the model under different threshold settings.

In Figure 11, we illustrate how the model’s performance changes with respect to the threshold  $\tau$ . It is observed that InfoBound achieves significant improvement in OoD SI-Accuracy and SI-Recall, while maintaining competitive performance in ID SI-Accuracy compared to SCONE. This consistent improvement observed across different threshold

values of  $\tau$  highlights InfoBound’s superiority and robustness in real-world scenarios. It ensures that a larger number of semantically in-distribution samples can be effectively incorporated into the classification process, reducing false positives while maintaining high classification accuracy on ID data. This improvement further solidifies the effectiveness of InfoBound in practical applications.

#### 4 Explanations for the Validity of Our Assumptions

In Figure 12, to validate the separability of covariate-shifted and semantic-shifted data in embedding space, we present the T-SNE visualization of the penultimate-layer feature embeddings from the pre-trained Wide ResNet model and the zero-shot CLIP model. It is observed that many semantic-shifted OoD data points are located farther from the ID data, whereas covariate-shifted data points are relatively

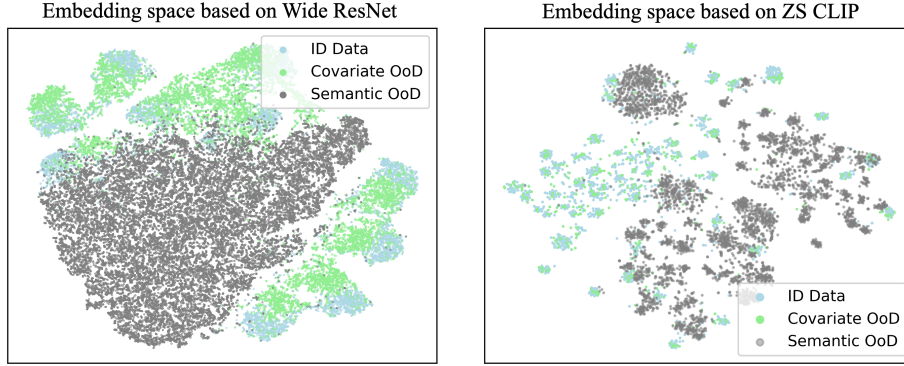


Fig. 12: T-SNE visualization of the initial state of the penultimate-layer feature embeddings. The result based on Wide ResNet is conducted on the mixture of the ID data (CIFAR-10), covariate-shifted OoD data (CIFAR-10-C), and semantic-shifted OoD data (SVHN). The result based on zero-shot (ZS) CLIP is conducted on the mixture of the ID data (40% classes from ImageNet-1K), covariate-shifted OoD data (the ImageNet-V2 subset that has the same class labels with ID data), and semantic-shifted OoD data (the other 60% classes from ImageNet-1K). Here, the result based on zero-shot (ZS) CLIP is obtained by randomly sampling instances from the original data for clearer visualization.

closer to the ID data. This observation indicates that useful information about semantic IN and semantic OUT can be inferred from the latent space of the unlabeled wild mixture. By leveraging the coarse separability of covariate-shifted and semantic-shifted data in the initial embedding space, the proposed InfoBound method effectively accesses information related to various distribution shifts. The method then refines the embedding distributions through the MI-Min and CE-Max processes, further enhancing its ability to distinguish between different types of OoD data.

In Figure 13, we provide empirical evidence supporting the reasonableness of the assumption in Proposition 1. For each sample from the covariate-shifted OoD and semantic-shifted OoD data, we compute its nearest Euclidean distance to the ID samples. The distribution of these nearest distances is presented in Figure 13. It is shown that there is a significant overlap between the distance distributions of covariate-shifted OoD and semantic-shifted OoD data, which suggests that there exist covariate-shifted and semantic-shifted data satisfying  $\|Z_{id} - Z_{c-out}\|_2 \leq \epsilon_0$  and  $\|Z_{id} - Z_{s-out}\|_2 \leq \epsilon_0$  for some  $\epsilon_0 > 0$ .

In Figure 14, we provide empirical evidence supporting the reasonableness of the assumption in Theorem 3. From the third column in Figure 14, where we take the OoD samples with the nearest distance to ID samples of approximately 0.3 as an example, we can observe that at different training steps, there exists a threshold  $\theta_0$  that successfully detects all the covariate-shifted OoD samples as semantic IN, while also correctly identifying a portion of the semantic-shifted OoD samples as semantic OUT.

### .5 Insights into SCONE’s Trade-off

SCONE is the first method to jointly address both OoD generalization and OoD detection in a unified framework. It introduces a margin-based approach that enhances generalization to covariate shifts while also enabling OoD detection for semantic shifts. However, despite its strong performance in OoD generalization, SCONE suffers from a noticeable drop in OoD detection. We explain the trade-off

in SCONE from two main aspects: 1) *The energy margin on ID data can unexpectedly influence nearby semantic-shifted OoD points (also known as hard OoD samples). The corresponding theoretical analysis is presented in Proposition 3.* 2) *As stated in the original paper, “SCONE aims to classify as many samples as possible from the mixture of unlabeled data as semantic OUT”. This optimization objective inherently increases the risk of confusion between different distributions. Furthermore, covariate-shifted and semantic-shifted data can exhibit significant overlap in the latent space. Although SCONE incorporates a margin constraint on ID data to prevent covariate-shifted samples from being misclassified as semantic OUT, its effectiveness diminishes when addressing such overlap, as demonstrated in Proposition 3. Consequently, this approach inevitably leads to degraded performances in distinguishing semantic-out from semantic-in samples.* These factors make it challenging to distinguish nearby semantic-shifted OoD samples from ID samples, ultimately resulting in significant performance degradation in OoD detection. Now, we delve into each reason and present the corresponding explanations as follows:

1) In the SCONE method, it was pointed out that “enforcing an energy margin on ID data has the effect of also lowering the energy of nearby covariate-shifted OoD points, which are semantically related to ID points. Since lower energy increases the value of the classifier logits, the covariate-OoD points then enjoy an increased logit in their correct classes, leading to stronger OoD generalization.” However, we discover that the energy margin on ID data not only affects nearby covariate-shifted OoD points but also unexpectedly influences nearby semantic-shifted OoD points (also known as hard OoD samples). As the margin decreases, the SCONE method improves OoD accuracy but simultaneously makes it more challenging to distinguish nearby semantic-shifted OoD samples from ID samples. This results in a trade-off between OoD generalization and OoD detection. We present the theoretical analysis in Proposition 3, which demonstrates that: if the margin  $\eta$  is sufficiently large to ensure that all covariate-shifted out-of-distribution (OoD) points are detected as semantic IN,

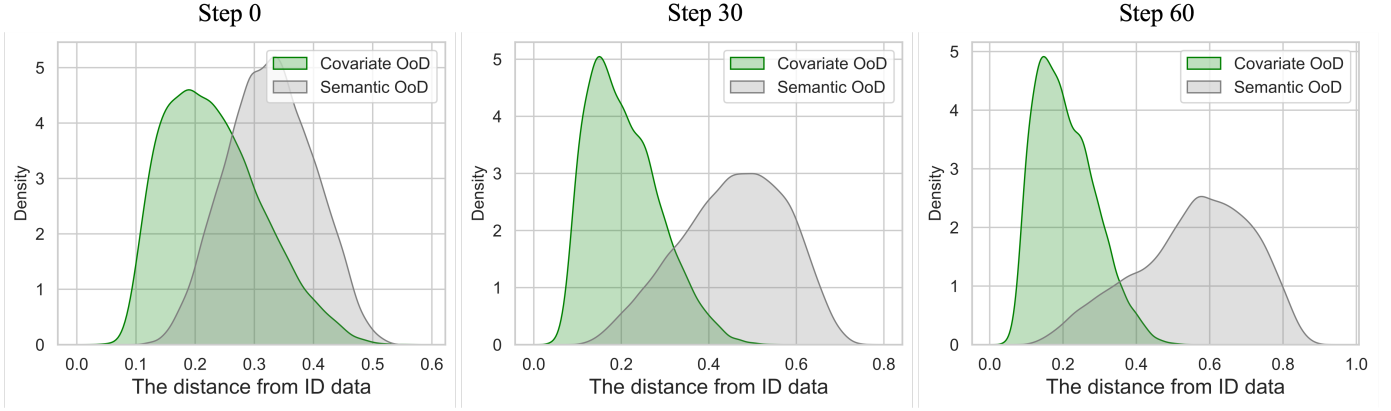


Fig. 13: Empirical evidence supporting the reasonableness of the assumption in Proposition 1. We present a visual comparison of the nearest distance distributions to the ID data at different training steps of InfoBound. At training step 0, which corresponds to the initial state of the pre-trained model, there is a significant overlap between the distance distributions of covariate-shifted OoD and semantic-shifted OoD data. However, as the InfoBound training progresses, it helps the semantic-shifted data move away from the ID data, which facilitates better distinction between semantic IN and semantic OoD.

it simultaneously leads to the misclassification of nearby semantic-shifted samples as semantic IN. Moreover, we present the T-SNE visualizations of ID samples and hard-to-distinguish semantic-shifted OoD samples under different SCONE margin values in Figure 15. The results show that as the margin in SCONE decreases, the overlap between the embedding distributions of ID samples and hard-to-distinguish semantic-shifted OoD samples consistently grows. This increased overlap leads to a significant degradation in OoD detection performance.

2) The SCONE method explicitly optimizes a binary classifier based on the energy function, aiming to classify as many samples as possible from the mixture of unlabeled data as semantic OoD. However, this optimization objective inevitably introduces confusion between different distributions, potentially leading to the misclassification of semantically shifted data—especially those close to covariate-shifted samples—as semantic IN. This issue is evidenced by the ablation study results on mixing ratio  $\pi_s$  in Table 13. The results indicate that as the ratio of semantic-shifted data decreases, classifying as many samples as possible from the wild data as semantic OoD leads to a significant performance drop in OoD detection. This demonstrates that the SCONE method is highly sensitive to mixing ratios. In other words, when semantic-shifted data is scarce in the unlabeled wild mixture—a common scenario in real-world applications—SCONE’s optimization objective may be insufficient to ensure robust OoD detection.

## .6 Proof of Lemma 1

**Lemma S1. [Restatement of Lemma 1]** Based on the definition in Equation 1, the mutual information  $I(Z_{s-in}; Z_{s-out})$  is upper bounded by:

$$\begin{aligned} I(Z_{s-in}; Z_{s-out}) &= \sum_{d=1}^D \sum_{d'=1}^D P_{dd'} \ln \frac{P_{dd'}}{P_d \cdot P_{d'}} \\ &\leq Z_{s-in} Z_{s-out}^T + \sum_{d=1}^D \sum_{d'=1}^D P_{dd'} I\{d \neq d'\} \end{aligned} \quad (14)$$

TABLE 13: Comparison with SCONE on different mixing ratios  $\pi_s$ . We train on CIFAR-10 as ID, using CIFAR-10-C as covariate-shifted data and SVHN as semantic-shifted data (with fixed  $\pi_c = 0.5$ ). Here,  $\pi_s$  and  $\pi_c$  denote the proportion of semantic-shifted unlabeled data and covariate-shifted unlabeled data in the wild mixture, respectively. For the SCONE [4] method, we set the margin as  $-10$  following its original paper.

SCONE \ $\pi_s$	0.1	0.15	0.2	0.25	0.3	0.35	0.4	0.45	0.5
OoD Acc $\uparrow$	84.69	82.26	82.26	82.01	81.77	81.72	81.51	81.35	81.08
ID Acc $\uparrow$	94.65	95.10	95.09	95.03	95.04	95.03	95.04	95.05	95.04
FPR $\downarrow$	10.86	12.52	10.25	9.26	8.32	7.62	7.31	7.04	6.63
AUROC $\uparrow$	97.84	97.58	98.05	98.23	98.42	98.57	98.63	98.71	98.77
InfoBound \ $\pi_s$	0.1	0.15	0.2	0.25	0.30	0.35	0.40	0.45	0.50
OoD Acc $\uparrow$	84.38	83.81	83.29	83.15	82.76	82.33	81.96	81.61	81.05
ID Acc $\uparrow$	94.70	94.62	94.62	94.54	94.47	94.39	94.34	94.39	94.40
FPR $\downarrow$	2.92	1.78	1.46	1.11	0.90	0.74	0.64	0.51	0.44
AUROC $\uparrow$	99.45	99.65	99.72	99.79	99.83	99.85	99.87	99.89	99.90

Proof:

$$\begin{aligned} I(Z_{s-in}; Z_{s-out}) &= \sum_{d=1}^D \sum_{d'=1}^D P_{dd'} \ln \frac{P_{dd'}}{P_d P_{d'}} \\ &\leq \sum_{d=1}^D \sum_{d'=1}^D P_{dd'} \left( \frac{P_{dd'}}{P_d P_{d'}} - 1 \right) \\ &= - \sum_{d=1}^D \sum_{d'=1}^D P_{dd'} + \sum_{d=1}^D \sum_{d'=1}^D \frac{P_{dd'}^2}{P_d P_{d'}} \end{aligned} \quad (15)$$

Let  $Z_{s-in} = [z_{11}, z_{12}, \dots, z_{1D}]$  and  $Z_{s-out} = [z_{21}, z_{22}, \dots, z_{2D}]$ , we denote the sum of all elements of  $Z_{s-in}$  and  $Z_{s-out}$  as  $s_1$  and  $s_2$  respectively, i.e.,  $s_1 = \sum_{j=1}^D z_{1j}$  and  $s_2 = \sum_{j=1}^D z_{2j}$ . After applying the softmax function to all representations, we have  $s_1 = s_2 = 1$ ,  $z_{1j} \geq 0$  and  $z_{2j} \geq 0$  for  $(j = 1, 2, \dots, D)$ . Then we can represent  $P_{dd'}$  and  $P_d P_{d'}$  as follows:

$$P_{dd'} = \frac{1}{2} (z_{1d} z_{2d'} + z_{2d} z_{1d'}) \quad (16)$$

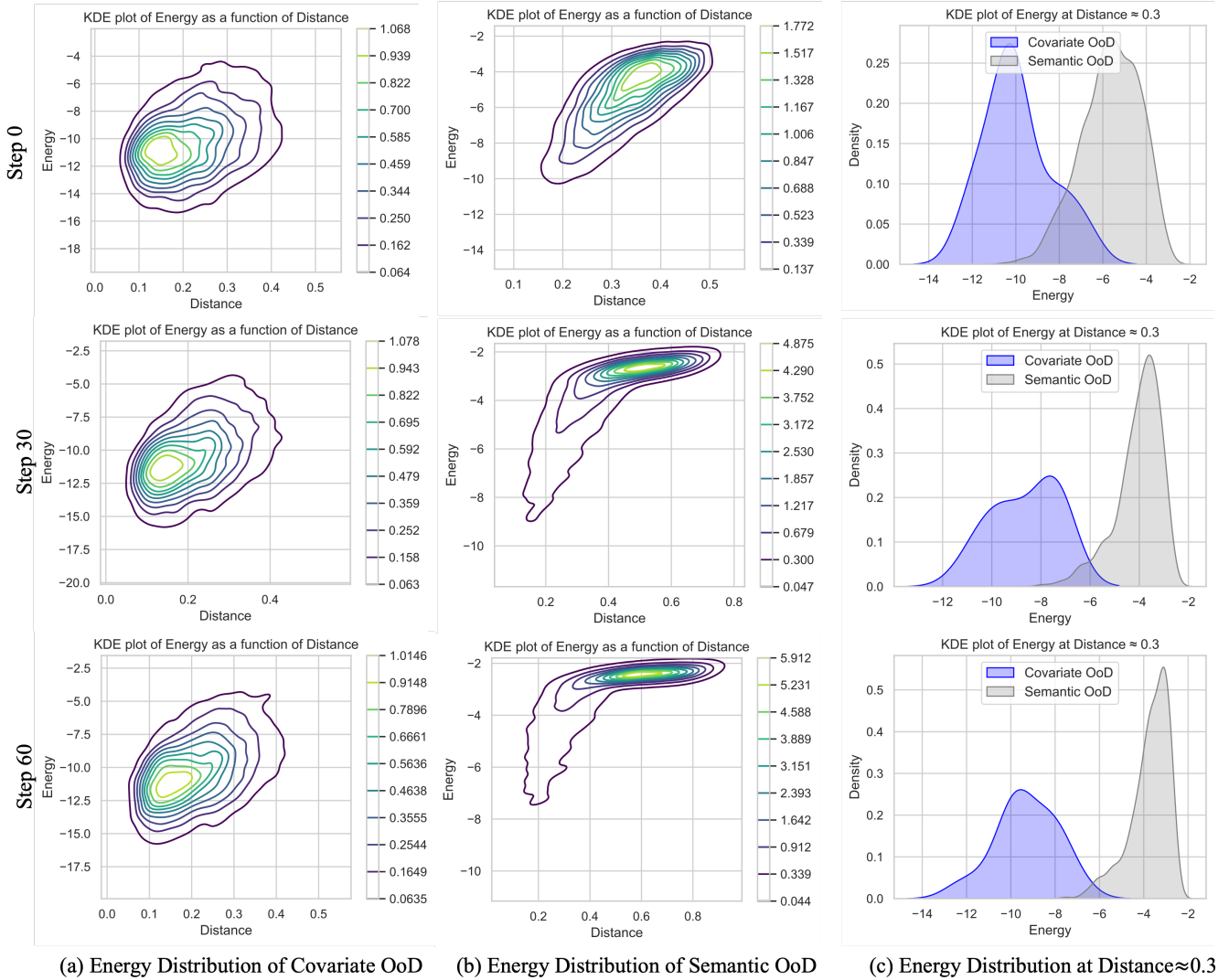


Fig. 14: Energy visualization for the covariate-shifted and semantic-shifted OoD data across different nearest distances to the ID data. We also present the energy distribution when the nearest distance between the OoD sample and the ID samples is approximately 0.3. From the second row in the figure, as InfoBound training progresses, the energy distribution of the semantic-shifted OoD data becomes more concentrated in the upper-right corner. This indicates that the latent features of semantic-shifted OoD move away from the semantic-in data (as a result of MI-Min), and the energy scores of semantic-shifted OoD gradually increase (as a result of CE-Max).

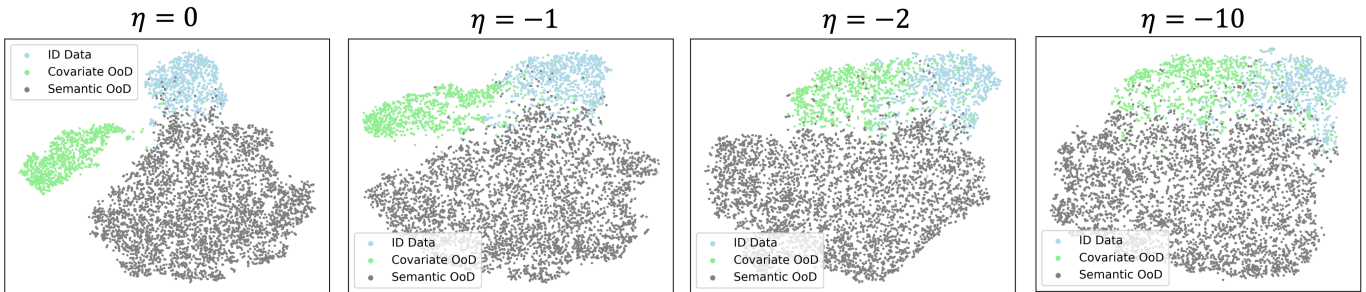


Fig. 15: T-SNE visualization of ID samples and hard-to-distinguish semantic-shifted OoD samples under different SCONE margin values. As the margin value decreases, the learned model pulls ID data and covariate-shifted OoD data closer. However, this comes at the cost of increased confusion between semantic-in and semantic-out data, significantly degrading OoD detection performance.

$$P_d = \sum_{d'=1}^D P_{dd'} = \frac{1}{2}(z_{1d}s_2 + z_{2d}s_1) \quad (17)$$

$$P_{d'} = \sum_{d=1}^D P_{dd'} = \frac{1}{2}(z_{1d'}s_2 + z_{2d'}s_1) \quad (18)$$

$$\begin{aligned} P_d P_{d'} &= \frac{1}{4}(z_{1d}s_2 + z_{2d}s_1)(z_{1d'}s_2 + z_{2d'}s_1) \\ &= \frac{1}{4}(z_{1d} + z_{2d})(z_{1d'} + z_{2d'}) \\ &= \frac{1}{4}(z_{1d}z_{2d'} + z_{2d}z_{1d'} + z_{1d}z_{1d'} + z_{2d}z_{2d'}) \end{aligned} \quad (19)$$

It is easy to know that  $P_{dd'} \leq 2P_d P_{d'}$ . Consequently, Equation 15 can be upper bounded as follows:

$$\begin{aligned} I(Z_{s\text{-in}}; Z_{s\text{-out}}) &\leq \sum_{d=1}^D \sum_{d'=1}^D P_{dd'} \\ &= \sum_{d=1}^D \sum_{d'=1}^D P_{dd'} I\{d = d'\} + \sum_{d=1}^D \sum_{d'=1}^D P_{dd'} I\{d \neq d'\} \quad (20) \\ &= Z_{s\text{-in}} Z_{s\text{-out}}^T + \sum_{d=1}^D \sum_{d'=1}^D P_{dd'} I\{d \neq d'\} \end{aligned}$$

Thus complete the proof.

## 7 Proof of Equation 4

Proof: In Section 3.1.1, we have constructed the optimization objective for the MI-Min process as follows:

$$\begin{aligned} \min \mathbb{E}[Z_{s\text{-in}} Z_{s\text{-out}}^T] &\implies \min \mathbb{E}[(Z_{id} Z_{s\text{-out}}^T)] \\ \text{s.t. } \mathbb{E} \left[ \log \frac{\exp(Z_{id} Z_{s\text{-out}}^T)}{\exp(Z_{id} Z_{c\text{-out}}^T)} \right] &= \min \mathbb{E} \left[ \log \frac{\exp(Z_{id} Z_{s\text{-out}}^T)}{\exp(Z_{id} Z_{c\text{-out}}^T)} \right] \end{aligned} \quad (21)$$

where  $\mathbb{E} \left[ \log \frac{\exp(Z_{id} Z_{s\text{-out}}^T)}{\exp(Z_{id} Z_{c\text{-out}}^T)} \right]$  is a random variable concerning the model parameters. Since all latent features are normalized by softmax, we have  $|\min \mathbb{E}[\log(\exp(Z_{id} Z_{s\text{-out}}^T) / \exp(Z_{id} Z_{c\text{-out}}^T))]| \leq 2$ . In other words, based on the optimization condition presented in Equation 21, there exists some  $\delta^*$  ( $-2 < \delta^* \leq 2$ ) such that:

$$\mathbb{E} \left[ \log \frac{\exp(Z_{id} Z_{s\text{-out}}^T)}{\exp(Z_{id} Z_{c\text{-out}}^T)} \right] - \delta^* \leq 0 \quad (22)$$

By implementing the Lagrange Multiplier method, with the Lagrange multiplier denoted as  $\alpha$ , ( $\alpha > 0$ ), the optimization objective as shown in Equation 21 can be reformulated as:

$$\begin{aligned} \mathcal{L} &= \mathbb{E}[Z_{id} Z_{s\text{-out}}^T] + \alpha \mathbb{E} \left[ \log \frac{\exp(Z_{id} Z_{s\text{-out}}^T)}{\exp(Z_{id} Z_{c\text{-out}}^T)} \right] - \alpha \delta^* \\ \implies \mathcal{L} &= (1 + \alpha) \mathbb{E}[Z_{id} Z_{s\text{-out}}^T] - \alpha \mathbb{E}[Z_{id} Z_{c\text{-out}}^T] \end{aligned} \quad (23)$$

Thus complete the proof.

## 8 Proof of Equation 7

Proof: Taking  $h(Z_{s\text{-out}})$  as an example, its entropy is calculated as:

$$H(h(Z_{s\text{-out}})) = - \sum_{j=1}^{n_3} \sum_{k=1}^C h_k(Z_{s\text{-out}}^j) \log h_k(Z_{s\text{-out}}^j) \quad (24)$$

where  $h_k(\cdot)$  denotes the  $k$ -th element of the output  $h(\cdot)$ .

The mathematical relationship between the energy function and the entropy of output logits is established through the concept of softmax, which is commonly used in machine learning for classification problems. To see this, we express the output logits as  $h(Z) = [h_1(Z), h_2(Z), \dots, h_C(Z)]$ , The output logits can be used to drive a categorical distribution using the softmax function:

$$h'_i = \frac{e^{h_i(Z)}}{\sum_{i=1}^C e^{h_i(Z)}} \quad (25)$$

Then the entropy can be calculated as:

$$\begin{aligned} \text{Entropy}(h) &\propto - \sum_{i=1}^C h'_i(Z) \log h'_i(Z) \\ &= - \sum_{i=1}^C \frac{e^{h_i(Z)}}{\sum_{i=1}^C e^{h_i(Z)}} \log \frac{e^{h_i(Z)}}{\sum_{i=1}^C e^{h_i(Z)}} \\ &= - \sum_{i=1}^C \frac{e^{h_i(Z)}}{\sum_{i=1}^C e^{h_i(Z)}} h_i + \log \sum_{i=1}^C e^{h_i(Z)} \\ &\geq - \frac{\sum_{i=1}^C e^{2h_i(Z)}}{e^{-E(h)}} \geq - \frac{(\sum_{i=1}^C e^{h_i(Z)})^2}{e^{-E(h)}} \\ &\geq -e^{-E(h)} \propto E(h) \end{aligned} \quad (26)$$

where  $E(h) = -\log \sum_{i=1}^C e^{h_i(Z)}$  is the energy score of the output logits  $h(Z)$ . Taking  $\min H(h(Z_{s\text{-in}}))$  into consideration, we formulate the optimization for  $\max H(h(Z_{s\text{-out}}) | h(Z_{s\text{-in}}))$  as the following energy-based loss function:

$$\begin{aligned} \mathcal{L}_{\text{CE-Max}} &= \sum_{i=1}^{n_3} \frac{1/n_3}{1 + \exp(\beta \cdot E(h(Z_{s\text{-out}}^i)))} \\ &+ \sum_{i=1}^{n_1+n_2} \frac{1/(n_1+n_2)}{1 + \exp(-\beta \cdot E(h(\hat{Z}_{s\text{-in}}^i)))} \end{aligned} \quad (27)$$

Thus complete the proof.

## 9 Proof of Proposition 1

**Proposition S1. [Restatement of Proposition 1]** Suppose there exist covariate-shifted and semantic-shifted data satisfying  $\|Z_{id} - Z_{c\text{-out}}\|_2 \leq \varepsilon_0$  and  $\|Z_{id} - Z_{s\text{-out}}\|_2 \leq \varepsilon_0$ . Assume that the classifier  $h$  is  $L$ -Lipschitz. We consider a binary classification task distinguishing between semantic IN and semantic OUT, where the classification boundary is defined by  $E(h(Z)) = 0$  and  $E(h(Z))$  is the energy of  $h(Z)$ . In the SCONE method, a margin  $\eta$  is incorporated for ID data. While setting  $\eta \leq -L\varepsilon_0$  allows covariate-shifted OoD points to be detected as semantic IN and increases the logit for their correct classes, it simultaneously results in all semantic-shifted samples satisfying  $\|Z_{id} - Z_{s\text{-out}}\|_2 \leq \varepsilon_0$  to be incorrectly detected as semantic IN.

Proof: Considering the two-class case with the final probability to be  $(h(Z), -h(Z))$ , the energy function becomes  $E(h(Z)) = -\log(e^{h(Z)} + e^{-h(Z)})$ . Since we assume that the classifier  $h$  is  $L$ -Lipschitz and  $-\log(e^u + e^{-u}) \leq |u|$ , we have:

$$-L\varepsilon_1 + E(h(Z_{id})) \leq E(h(Z_{c\text{-out}})) \leq L\varepsilon_1 + E(h(Z_{id})) \quad (28)$$

Then incorporating a margin  $\eta$  on ID data results in the following bounds:

$$E(h(Z_{c-out})) \leq \eta + L\varepsilon_0 \quad \text{and} \quad E(h(Z_{s-out})) \leq \eta + L\varepsilon_0.$$

If  $\eta \leq -L\varepsilon_0$ , then all covariate-shifted samples satisfying  $\|Z_{id} - Z_{c-out}\|_2 \leq \varepsilon_0$  would be correctly detected as semantic IN. Since lower energy increases the value of the classifier logits, the covariate-shifted OoD points then enjoy an increased logit in their correct classes, leading to stronger OoD generalization. However, this comes at the cost of incorrectly detecting all semantic-shifted samples satisfying  $\|Z_{id} - Z_{s-out}\|_2 \leq \varepsilon_0$  as semantic IN. Thus, complete the proof of SCONE's margin leads to trade-offs between OoD generalization and OoD detection.

## 10 Proof of Theorem 1

**Theorem S1. [Restatement of Theorem 1]** *Given the ID training data  $(X_{id}, Y)$  sampling from the ID distribution  $\mathcal{D}_{id}$ , and the freely available unlabeled covariate-shifted OoD data  $X_{c-out}$  from distribution  $\mathcal{D}_{c-out}$  and unlabeled semantic-shifted OoD data  $X_{s-out}$  from distribution  $\mathcal{D}_{s-out}$ , we train the proposed InfoBound model and we denote parameters in the converged InfoBound model as  $\omega_{\text{InfoBound}}^\infty$ . Keeping the model architecture unchanged but replacing the optimization objective with empirical risk minimization (ERM), we denote the model parameters of the ERM model at training step  $t$  as  $\omega_{\text{ERM}}^t$ . Thus, we denote the InfoBound model as  $f_{\text{InfoBound}}(X; \omega_{\text{InfoBound}}^\infty)$  and denote the ERM model at training step  $t$  as  $f_{\text{ERM}}(X; \omega_{\text{ERM}}^t)$ , ( $t \in [0, +\infty)$ ). Based on the square loss function  $\ell$ , we define InfoBound's prediction errors on covariate-shifted OoD data as:*

$$\begin{aligned} \mathcal{L}_{c-out}(f_{\text{InfoBound}}(\omega_{\text{InfoBound}}^\infty)) &:= \\ &\mathbb{E}_{(X,Y) \in \mathcal{D}_{c-out}} [\ell(f_{\text{InfoBound}}(X; \omega_{\text{InfoBound}}^\infty), Y)], \end{aligned} \quad (29)$$

and the ERM model's prediction errors as:

$$\mathcal{L}_{c-out}(f_{\text{ERM}}(\omega_{\text{ERM}}^t)) := \mathbb{E}_{(X,Y) \in \mathcal{D}_{c-out}} [\ell(f_{\text{ERM}}(X; \omega_{\text{ERM}}^t), Y)].$$

Then for  $\forall \delta > 0$  and  $\forall t > 0$ , the prediction errors of InfoBound and ERM satisfy:

$$\mathbb{P} \left( \frac{\mathcal{L}_{c-out}(f_{\text{InfoBound}}(\omega_{\text{InfoBound}}^\infty))}{\min_{t>0} \mathcal{L}_{c-out}(f_{\text{ERM}}(\omega_{\text{ERM}}^t))} \geq \delta \right) = 0 \quad (30)$$

**Proof:** Without loss of generality, we elaborate on the binary classification case, which is easy to generalize to multi-label classification. For clarity, we first state some important notations as follows:

**Notation 2.** *Given the labeled training sets  $\{(X, Y), X \in \mathbb{R}^{1 \times D_0}, Y \in \{0, 1\}\}$  from the training domain (source domain)  $\mathcal{D}_{id}$ , we focus on the task of training models with the expectation that they perform well on the covariate-shifted OoD data. The covariate-shifted OoD data is sampled from the unseen target domain, denoted as  $\mathcal{D}_{c-out}$ . In this paper, we consider the model to be composed of a model backbone and a classifier head. All model parameters that need to be learned include  $\omega := \{V, W\}$ , where  $V \in \mathbb{R}^{D_0 \times D}$  denotes the parameter of model backbone and  $W \in \mathbb{R}^{D \times 1}$  denotes the parameter of classifier head. Then the model's generic form is given by  $Y = V^\top XW$ , where the predicted probability over the positive class ( $Y = 1$ ) can be obtained using sigmoid activation. In the proposed InfoBound*

*method, we manipulate the distribution of representations. We denote the representation as  $Z \in \mathbb{R}^{1 \times D}$ ,  $Z = V^\top X$ . As in prior work [93], we make the assumption that the initialization and optimal values of the model parameter  $V$  have been orthogonalized, resulting in orthogonal columns. For the classifier's weight  $W$ , we assume that  $\|W\|_2 = 1$ . We also assume the input  $X$  is  $L_2$  normalized. The optimal solution of model  $Y = V^\top XW$  is denoted as  $\omega^* = \{V^*, W^*\}$ . Correspondingly, the maximum singular value of  $V^*$  is set such that  $\sigma_{\max}(V^*) = \sqrt{D}$ .*

Assuming that we have achieved an optimization state where the proposed MI-Min loss is no more than  $\eta$ , i.e.,  $\mathcal{L}_{\text{MI-Min}} \leq \eta$ , and the mean square error by  $Y = V^\top XW$  is less than  $\varepsilon'$ , i.e.,  $\mathbb{E}_{(Z_{id}, Y) \sim \mathcal{D}_{id}} \|Z_{id}W - Y\|_2^2 \leq \varepsilon'$ . The corresponding model parameter in InfoBound is denoted as  $\omega_{\text{InfoBound}}$ . Under the model assumption that the softmax function is stacked at the layer preceding the MI-Min process, the value of  $\eta$  is constrained such that  $|\eta| \leq 2$ . Let  $\varepsilon_1 = 2\sqrt{2 - |\eta|}$ , we can deduce the following relationship:

$$\|Z_{id} - Z_{c-out}\|_2 \leq \varepsilon_1 \quad (31)$$

Then the prediction errors on covariate-shifted OoD data,  $(X, Y) \in \mathcal{D}_{c-out}$ , obtained by the proposed InfoBound method can be calculated as:

$$\begin{aligned} \mathcal{L}_{c-out}(f_{\text{InfoBound}}(\omega_{\text{InfoBound}}^\infty)) &= \mathbb{E}_{\mathcal{D}_{c-out}} [\ell(f_{\text{InfoBound}}(X; \omega_{\text{InfoBound}}^\infty), Y)] \\ &= \mathbb{E}_{\mathcal{D}_{c-out}} \|Z_{c-out}W - \mathbb{E}_{\mathcal{D}_{id}}[Z_{id}W] + \mathbb{E}_{\mathcal{D}_{id}}[Z_{id}W] - Y\|_2^2 \\ &\leq \mathbb{E}_{\mathcal{D}_{c-out}} \mathbb{E}_{\mathcal{D}_{id}} \|Z_{c-out}W - Z_{id}W\|^2 + \mathbb{E}_{\mathcal{D}_{id}} \|Z_{id}W - Y\|_2^2 \\ &\leq \mathbb{E}_{\mathcal{D}_{c-out}} \|W\|_2^2 \|Z_{c-out} - Z_{id}\|_2^2 + \varepsilon' \leq (\varepsilon_1 + \varepsilon') \end{aligned} \quad (32)$$

Before discussing the lower bound of ERM's prediction errors on covariate-shifted OoD data, let's start by introducing a useful property.

**Lemma S2.** *We denote the optimal solution of model  $Y = V^\top XW$  as  $\omega^* = \{V^*, W^*\}$ . With  $W$  leaned by the proposed InfoBound frozen, if  $W$  satisfies the mean square error by  $Y = V^\top XW$  is less than  $\varepsilon'$ , i.e.,  $\mathbb{E}\|X(VW - V^*W^*)\|_2^2 \leq \varepsilon'$ , then  $\exists c_w \geq 0$  and  $\exists c_v \geq 0$  such that  $\|W - W^*\|_2^2 \leq \varepsilon_w$  and  $\|V - V^*\|_F^2 \leq \varepsilon_v$ , where  $\varepsilon_w = c_w \varepsilon'$  and  $\varepsilon_v = c_v \varepsilon'$ .*

**Proof:** By simple algebraic manipulation, we get:

$$\begin{aligned} &\mathbb{E}\|X(VW - V^*W^*)\|_2^2 \\ &= \mathbb{E}\|X(V^*W - V^*W^* + VW - V^*W)\|_2^2 \\ &\leq \mathbb{E}\|X(V^*W - V^*W^*)\|_2^2 + \mathbb{E}\|X(VW - V^*W)\|_2^2 \\ &\leq \mathbb{E}\|XV^*\|_2^2 \|(W - W^*)\|_2^2 + \mathbb{E}\|XW\|_2^2 \|(V - V^*)\|_F^2 \\ &\leq \mathbb{E}[\sigma_{\max}^2(V^*) \|(W - W^*)\|_2^2] + \mathbb{E}\|X\|_2^2 \|W\|_2^2 \|(V - V^*)\|_F^2 \\ &\leq D \|(W - W^*)\|_2^2 + \|(V - V^*)\|_F^2 \leq \varepsilon' \end{aligned} \quad (33)$$

We can take  $c_w = 1/D$  and  $c_v = 1$ , and then the expressions  $\|W - W^*\|_2^2 \leq \varepsilon_w$  and  $\|V - V^*\|_F^2 \leq \varepsilon_v$  are established. Thus complete the proof.

Now, we calculate the lower bound of ERM's prediction errors on covariate-shifted OoD data.

**Theorem S2. [Upper Bound of the Prediction Errors by ERM]** *Based on the model setting and data assumptions defined in Assumption 1 and Notations 2, we denote the model parameter leaned by the proposed InfoBound, denoted as  $\omega_{\text{InfoBound}} =$*

$\{V, W\}$ . For the ERM model, we initialize the model parameter as  $\omega_{\text{InfoBound}}$ , which satisfies  $\mathbb{E}\|Z_{\text{id}}(W - W^*)\|_2^2 \leq \varepsilon'$ . Then  $\exists \varepsilon_w > 0$  and  $\exists \varepsilon_v > 0$  such that  $\|W - W^*\|_2^2 \leq \varepsilon_w$  and  $\|V - V^*\|_F^2 \leq \varepsilon_v$ , and the prediction errors on covariate-shifted data by the ERM model, represented as  $\mathcal{L}_{c\text{-out}}(f_{\text{ERM}}(\omega_{\text{ERM}}^\infty))$ , is lower bounded by:

$$2\sigma_{\min}(\Sigma)(\min\{O(\phi), O((\phi^2 - \varepsilon'^2 - \varepsilon_w^2 - \varepsilon'_v \varepsilon_w)/\varepsilon_w)\})^2 \quad (34)$$

where  $\Sigma = \mathbb{E}(X^\top X)$  and  $\phi^2 = \|W^{*\top} W^*\|_2$ .

Note that the Big-O notation  $O(\cdot)$  means the asymptotic upper bound on the order of magnitude of a function described by another (usually simpler) function.

Proof: We denote the converged solution for the model parameter under ERM as  $\omega^\infty = \{V^\infty, W^\infty\}$ , denote the solution at step  $t$  under ERM as  $\omega_t = \{V_t, W_t\}$ . The prediction errors on covariate-shifted data by the ERM model ( $Y = V^\top XW$ ) can be computed as:

$$\begin{aligned} & \mathcal{L}_{c\text{-out}}(f_{\text{ERM}}(\omega^\infty)) \\ &= (V^\infty W^\infty - V^* W^*)^\top \Sigma (V^\infty W^\infty - V^* W^*) \quad (35) \\ &\geq 2\sigma_{\min}(\Sigma) \|V^\infty W^\infty - V^* W^*\|_2^2 \end{aligned}$$

where  $\Sigma = \mathbb{E}(X^\top X)$  and  $\sigma_{\min}(\Sigma)$  is the minimum singular value of  $\Sigma$ . So it suffices to lower bound  $\|V_t W_t - V^* W^*\|_2^2$ .

Inspired by the proof technique in [93], we first assume that  $\|V^* W^* - V^\infty W^\infty\|_2 \leq \Delta$ , and we will show that:

$$\|(W^{*\top} W^*)^2 - (W_t^\top W^*)^2\|_2 \leq p(\Delta) \quad (36)$$

where  $p(\cdot)$  denotes the polynomial function corresponding to  $\Delta$ .

**First, we show**  $\|W_t - W^*\|_2 \leq \varepsilon_w/c$ .

We assume that the covariate factor  $Z_c$  from training sets is orthogonal to the covariate factor  $Z'_c$  from the OoD test sets. Let  $z = \frac{c}{\|W_t - W^*\|_2} (W_t - W^*)$ , then  $\exists y \in \mathbb{R}^{D_0 \times D}$  and its row vector  $y_i$ , s.t.  $y_i \in \mathcal{R}_0 = \text{rowspace}(V^\top X)$ . In the overparameterized model setting of DNNs, i.e.,  $D_0 > D$ , we can find a  $x \in \mathbb{R}^{D \times D}$  such that its row vector  $x_i \in \text{rowspace}(Z'_c)$  with  $\|x\|_F \leq 1$  and  $\Pi_{\mathcal{R}_0}(x) = y_i$  ( $\Pi_{\mathcal{R}_0}(x)$  denotes the projection of  $x$  on  $\mathcal{R}_0$ ). And we have  $xW = z$ . Since  $x$  is sampled from the space orthogonal to the subspace that training sets live in,  $V$  and  $W$  do not change in the directions of  $x$  when we learn the model on training data, so we have  $xW = xW_t$ .

The claim below follows simple algebraic manipulation, following the intuition we described.

$$\begin{aligned} \|W_t - W^*\|_2 &= \frac{1}{c} (W_t - W^*)^\top \frac{c(W_t - W^*)}{\|W_t - W^*\|_2} \\ &= \frac{1}{c} (W_t - W^*)^\top z \\ &= \frac{1}{c} (W_t - W^*)^\top xW \\ &= \frac{1}{c} x^\top W^\top W - x^\top W^\top W^* \\ &\leq \frac{1}{c} \|x\|_F \|W^\top W - W^\top W^*\|_2 \\ &\leq \frac{1}{c} \|W\|_2 \|W - W^*\|_2 \end{aligned} \quad (37)$$

As in prior work [93], we assume the initialization  $W$  has been  $L2$  normalized, i.e.,  $\|W\|_2 \leq 1$ . Therefore, we have:

$$\|W_t - W^*\|_2 \leq \varepsilon_w/c \quad (38)$$

**Then, we bound**  $\|VW^* - V_t W^*\|_2$ .

$$\begin{aligned} & \|VW^* - V_t W^*\|_2 \\ &\leq \|VW^* - V^* W^*\|_2 + \|V^* W^* - V_t W^*\|_2 \\ &\leq \|W^*\|_2^2 \|V - V^*\|_F \\ &\quad + \|V^* W^* + V_t W_t - V_t W_t - V_t W^*\|_2 \\ &\leq \|V - V^*\|_F + \|V^* W^* - V_t W_t\|_2 \\ &\quad + \|V_t W_t - V_t W^*\|_2 \end{aligned} \quad (39)$$

where the optimal solution  $W^*$  is  $L2$  normalized, i.e.,  $\|W^*\|_2 \leq 1$ .

As  $t \rightarrow \infty$ , incorporating Equation 38 into Equation 39, we get:

$$\|VW^* - V_t W^*\|_2 \leq \Delta + \varepsilon_v + \sigma_{\max}(V_t) \varepsilon_w/c = \Delta_1 \quad (40)$$

**Next, we compute**  $\|(W^{*\top} W^*)^2 - (W^\top W^*)^2\|_2$ .

By the triangle Inequality, we have:

$$\begin{aligned} & \|(W^{*\top} W^*)^2 - (W^\top W^*)^2\|_2 \\ &\leq \|(W^{*\top} W^*)^2 - (W_t^\top W^*)^2\|_2 \\ &\quad + \|(W_t^\top W^*)^2 - (W^\top W^*)^2\|_2 \end{aligned} \quad (41)$$

The first term in the RHS of Equation 41 can be bounded by:

$$\begin{aligned} & \|(W^{*\top} W^*)^2 - (W_t^\top W^*)^2\|_2 \\ &\leq \|(W^* + W_t)^\top (W^* - W_t)\|_2 \|W^{*\top} W^*\|_2^2 \\ &= \|(2W^* + W_t - W^*)^\top (W^* - W_t)\|_2 \|W^{*\top} W^*\|_2^2 \\ &\leq \|(2W^* + W_t - W^*)\|_2 \|(W^* - W_t)\|_2 \|W^{*\top} W^*\|_2^2 \\ &\leq [2\|W^*\|_2 + \|(W_t - W^*)\|_2] \|(W^* - W_t)\|_2 \|W^{*\top} W^*\|_2^2 \\ &= (\varepsilon_w/c)(2 + (\varepsilon_w/c)) := \Delta_2 \end{aligned} \quad (42)$$

Again since we have the following expression established according to [93]:

$$W_t W_t^\top - W W^\top = V_t^\top V_t - V^\top V \quad (43)$$

We conduct left multiply both sides by  $W^{*\top}$  and right multiply both sides by  $W^*$  to get:

$$(W^{*\top} W_t)^2 - (W^{*\top} W)^2 = \|W^{*\top} V_t^\top\|_2^2 - \|W^{*\top} V^\top\|_2^2 \quad (44)$$

And then the second term on the RHS of Equation 41 is bounded by:

$$\begin{aligned} & \|(W_t^\top W^*)^2 - (W^\top W^*)^2\|_2 = |\|V_t W^*\|_2^2 - \|V W^*\|_2^2| \\ &\leq \|V_t W^* - V W^*\|_2 \|V_t W^* + V W^*\|_2 \\ &\leq \Delta_1 \|2V W^* + V_t W^* - V W^*\|_2 \\ &\leq \Delta_1 (2\|V W^*\|_2 + \|V_t W^* - V W^*\|_2) \\ &\leq \Delta_1 (2\|V W^* - V^* W^*\|_2 + 2\|V^* W^*\|_2 + \Delta_1) \\ &\leq \Delta_1 (2\varepsilon_v + 2\sigma_{\max}(V^*) + \Delta_1) \\ &\leq \Delta_1 (2\varepsilon_v + 2D + \Delta_1) := \Delta_3 \end{aligned} \quad (45)$$

Now, we can bound  $|(W^{*\top} W^*)^2 - (W^\top W^*)^2|$  by:

$$\|(W^{*\top} W^*)^2 - (W^\top W^*)^2\|_2 \leq \Delta_2 + \Delta_3 \quad (46)$$

**Finally, we rewrite the bound above in terms of  $\Delta$ ,  $\varepsilon_w$  and  $\varepsilon_v$ .**



We recall that:

$$\Delta_1 = \Delta + \varepsilon_v + \sigma_{\max}(V_t)\varepsilon_w/c \quad (47)$$

$$\Delta_2 = (\varepsilon_w/c)(2 + (\varepsilon_w/c)) \quad (48)$$

$$\Delta_3 = \Delta_1(2\varepsilon_v + 2D + \Delta_1) \quad (49)$$

Plugging  $\Delta_1$  into  $\Delta_3$  and applying Big-Oh notation, we have:

$$\begin{aligned} \Delta_2 + \Delta_3 &= O(\Delta^2) + O(\Delta) + O(\varepsilon_w) + O(\varepsilon_v) \\ &+ O(\varepsilon_w\Delta) + O(\varepsilon_v\Delta) \\ &+ O(\varepsilon_w^2) + O(\varepsilon_v^2) + O(\varepsilon_w\varepsilon_v) \end{aligned} \quad (50)$$

Therefore, we obtain the lower bound of  $\|(W^{*\top}W^*)^2 - (W^\top W^*)^2\|_2$ :

$$\begin{aligned} &\|(W^{*\top}W^*)^2 - (W^\top W^*)^2\|_2 \\ &\leq O(\Delta^2) + O(\Delta) + O(\varepsilon_w) + O(\varepsilon_v) + O(\varepsilon_w\Delta) \\ &+ O(\varepsilon_v\Delta) + O(\varepsilon_w^2) + O(\varepsilon_v^2) + O(\varepsilon_w\varepsilon_v) \end{aligned} \quad (51)$$

**The final step is taking the contrapositive.**

We have shown that if  $\|V^{*\top}W^{*\top} - V^\infty W^\infty\|_F \leq \Delta$ , then Equation 51 holds. According to the contrapositive statement we analyzed above and the notation:

$$\begin{aligned} \Delta &= \min\{O(\phi), O(\phi^2 - O(\varepsilon_w) - O(\varepsilon_v) \\ &- O(\varepsilon_w^2) - O(\varepsilon_v^2) - O(\varepsilon_w\varepsilon_v))/(O(\varepsilon_w) + O(\varepsilon_v))\} \end{aligned} \quad (52)$$

if the inequality below holds:

$$\begin{aligned} &\|(W^{*\top}W^*)^2 - (W^\top W^*)^2\|_2 \\ &\geq O(\Delta^2) + O(\Delta) + O(\varepsilon_w) + O(\varepsilon_v) + O(\varepsilon_w\Delta) \\ &+ O(\varepsilon_v\Delta) + O(\varepsilon_w^2) + O(\varepsilon_v^2) + O(\varepsilon_w\varepsilon_v) \end{aligned} \quad (53)$$

then we have  $\|V^{*\top}W^{*\top} - V^\infty W^\infty\|_2 \geq \Delta$ .

That is, let  $\|(W^{*\top}W^*)^2 - (W^\top W^*)^2\|_2 = \phi^2 + \phi$  for some  $\phi > 0$ , Equation 53 is established under the condition as shown in Equation 52, so we have  $\|V^{*\top}W^{*\top} - V^\infty W^\infty\|_2$  is lower bounded by  $\Delta$ .

Based on Equation 35, since  $\sigma_{\min}(\Sigma)$  has a lower bound almost surely, the prediction error on the covariate-shifted data by the ERM model is lower bounded by:

$$\begin{aligned} \mathcal{L}_{\text{c-out}}(f_{\text{ERM}}(V^\infty, W^\infty)) &\geq 2\sigma_{\min}(\Sigma) \\ (\min\{O(\phi), O(\phi^2 - O(\varepsilon_w) - O(\varepsilon_v) - O(\varepsilon_w^2) \\ &- O(\varepsilon_v^2) - O(\varepsilon_w\varepsilon_v))/(O(\varepsilon_w) + O(\varepsilon_v))\})^2 \\ &= O(1/(\varepsilon_v + \varepsilon_w)^2) \end{aligned} \quad (54)$$

According to Theorem S2, it is easy to get that: as  $\delta = O(\varepsilon_v + \varepsilon_w) + O(\varepsilon_1) = O(\varepsilon') + O(\varepsilon_1) \rightarrow 0$ ,

$$\frac{\mathcal{L}_{\text{c-out}}(f_{\text{InfoBound}}(\omega_{\text{InfoBound}}^\infty))}{\min_{t>0} \mathcal{L}_{\text{c-out}}(f_{\text{ERM}}(\omega_{\text{ERM}}^t))} \leq \frac{c'\delta}{O(1/\delta^2)} \rightarrow 0 \quad (55)$$

That is when the proposed InfoBound converged on the training domains, we have as  $\varepsilon' + \varepsilon_1 \rightarrow 0$ ,

$$\mathbb{P}\left(\frac{\mathcal{L}_{\text{c-out}}(f_{\text{InfoBound}}(\omega_{\text{InfoBound}}^\infty))}{\min_{t>0} \mathcal{L}_{\text{c-out}}(f_{\text{ERM}}(\omega_{\text{ERM}}^t))} \geq \delta\right) = 0 \quad (56)$$

Thus complete the proof for Theorem 1.

## .11 Proof of Theorem 2

**Theorem S3. [Restatement of Theorem 2]** Suppose that the classifier  $h$  is  $L$ -Lipschitz. Under the loss function defined in Equation 5 and Equation 7, the training process of InfoBound satisfies the conditions of  $\mathcal{L}_{\text{MI-Min}} \leq \varepsilon_m$ , and  $\mathcal{L}_{\text{CE-Max}} \leq \varepsilon_c$  after training. Considering the binary classification for semantic IN and semantic OoD, with  $E(h(Z)) = 0$  as the classification boundary, if  $\varepsilon_c \leq (1 + e^{2\beta L\sqrt{2-|\varepsilon_m|}})^{-1}$ , then any ID sample satisfying  $E(h(Z_{\text{id}})) \leq -\frac{1}{\beta} \log(\frac{1}{\varepsilon_c} - 1)$ , will have its covariate-shifted OoD counterpart detected as semantic IN. Meanwhile, the mean energy score of identified semantic-shifted OoD samples is lower-bounded by  $\mathbb{E}_{Z_{\text{s-out}}}[E(h(\hat{Z}_{\text{s-out}}))] \geq 2L\sqrt{2-|\varepsilon_m|}$ .

Proof: Let  $h_i(Z)$  denote the  $i$ -th element of the final classification result  $h(Z)$ , let  $C$  denote the class number. Considering the two-class case with the final probability to be  $(h(Z), -h(Z))$ , the energy function becomes  $E(h(Z)) = -\log(e^{h(Z)} + e^{-h(Z)})$ . Assuming that we have achieved an optimization state where the proposed MI-Min loss is no more than  $\eta$ , i.e.,  $\mathcal{L}_{\text{MI-Min}} \leq \varepsilon_m$ . Under the model assumption that a softmax function is stacked at the layer preceding the MI-Min process, the value of  $\varepsilon_m$  is constrained such that  $|\varepsilon_m| \leq 2$ . Let  $\varepsilon_1 = 2\sqrt{2-|\varepsilon_m|}$ , then we can deduce the following relationship:

$$\|Z_{\text{id}} - Z_{\text{c-out}}\|_2 \leq \varepsilon_1 \quad (57)$$

Suppose that  $h$  is  $L$ -Lipschitz: this is the case for many classifier functions, such as two-layer ReLU networks with bounded variation. Then the energy score of  $Z_{\text{c-out}}$  satisfies:

$$-L\varepsilon_1 + E(h(Z_{\text{id}})) \leq E(h(Z_{\text{c-out}})) \leq L\varepsilon_1 + E(h(Z_{\text{id}})) \quad (58)$$

If the upper bound of  $E(h(Z_{\text{c-out}}))$  is smaller than zero, that is:

$$L\varepsilon_1 + E(h(Z_{\text{id}})) < 0 \quad (59)$$

$$\iff E(h(Z_{\text{id}})) < -2L\sqrt{2-|\varepsilon_m|} \quad (60)$$

then any ID sample or covariate-shifted OoD sample would be detected as semantic IN.

Again since  $\mathcal{L}_{\text{CE-Max}} < \varepsilon_c$ , we have the following inequality:

$$E(h(\hat{Z}_{\text{s-in}})) \leq -\frac{1}{\beta} \log\left(\frac{1}{\varepsilon_c} - 1\right) \quad (61)$$

$$E(h(\hat{Z}_{\text{s-out}})) \geq \frac{1}{\beta} \log\left(\frac{1}{\varepsilon_c} - 1\right) \quad (62)$$

where  $\hat{Z}_{\text{s-in}} = \{Z_{\text{id}}, Z_{\text{c-out}}\}$ . When the CE-Max's optimization result as shown in Equation 61 satisfies Equation 60:

$$-\frac{1}{\beta} \log\left(\frac{1}{\varepsilon_c} - 1\right) \leq -2L\sqrt{2-|\varepsilon_m|} \quad (63)$$

$$\iff \varepsilon_c \leq \frac{1}{1 + e^{2\beta L\sqrt{2-|\varepsilon_m|}}} \quad (64)$$

Thus, if  $\varepsilon_c \leq (1 + e^{2\beta L\sqrt{2-|\varepsilon_m|}})^{-1}$ , then any ID sample satisfying  $E(h(Z_{\text{id}})) \leq -\frac{1}{\beta} \log(\frac{1}{\varepsilon_c} - 1)$ , will have its covariate-shifted OoD counterpart detected as semantic IN. Meanwhile, the mean energy score of identified semantic-shifted OoD samples is lower-bounded by  $\mathbb{E}_{Z_{\text{s-out}}}[E(h(\hat{Z}_{\text{s-out}}))] \geq 2L\sqrt{2-|\varepsilon_m|}$ .

**.12 Proof of Theorem 3**

**Theorem S4. [Restatement of Theorem 3]** *Suppose there exist covariate-shifted and semantic-shifted samples such that their embeddings satisfy  $\|Z_{id} - Z_{c-out}\|_2 \leq \varepsilon_0$  and  $\|Z_{id} - Z_{s-out}\|_2 \leq \varepsilon_0$ . Based on the energy score, we assume there exists a threshold  $\theta_0$  that can detect all the covariate-shifted OoD samples as semantic IN while correctly identifying a portion of the semantic-shifted OoD samples as semantic OUT. If InfoBound satisfies the condition of  $\mathcal{L}_{CE-Max} \leq \varepsilon_c$  after training, then the false positive rate (FPR) of InfoBound on the semantic-shifted data, denoted as  $FPR_{\text{Infbound}}(Z_{s-out})$  is lower than that of SCONE, denoted as  $FPR_{\text{SCONE}}(Z_{s-out})$ , i.e.,  $FPR_{\text{Infbound}}(Z_{s-out}) < FPR_{\text{SCONE}}(Z_{s-out})$ .*

**Proof:** In the proposed InfoBound method, the energy scores of the identified semantic-shifted OoD samples satisfy:

$$\mathbb{E}_{Z_{s-out}} [E(h(Z_{s-out}))] \geq \frac{1}{\beta} \log\left(\frac{1}{\varepsilon_c} - 1\right) > 0.$$

Therefore, InfoBound’s false positive rate (FPR) on the semantic-shifted data from  $\|Z_{id} - Z_{s-out}\|_2 \leq \varepsilon'$  is lower than that of SCONE, i.e.,  $FPR_{\text{Infbound}}(Z_{s-out}) < FPR_{\text{SCONE}}(Z_{s-out})$ .

This theorem indicates that: under the condition that all the covariate-shifted OoD data detected as semantic IN, the SCONE method simultaneously classifies semantic-shifted OoD samples, whose nearest distance to the ID data is no larger than that of covariate-shifted OoD, as semantic IN. In contrast, our method can more effectively distinguish between semantic OoD and covariate OoD samples with the same nearest distance, resulting in a lower False Positive Rate (FPR) compared to SCONE.